

# 000 001 002 003 004 005 xLSTM SCALING LAWS: COMPETITIVE 006 PERFORMANCE WITH LINEAR TIME-COMPLEXITY 007 008 009

010 **Anonymous authors**  
011 Paper under double-blind review  
012  
013  
014  
015  
016  
017  
018  
019  
020  
021  
022  
023  
024  
025

## ABSTRACT

026 Scaling laws play a central role in the success of Large Language Models (LLMs),  
027 enabling the prediction of model performance relative to compute budgets prior to  
028 training. While Transformers have been the dominant architecture, recent alterna-  
029 tives such as xLSTM offer linear complexity with respect to context length while  
030 remaining competitive in the billion-parameter regime. We conduct a comparative  
031 investigation on the scaling behavior of Transformers and xLSTM along the follow-  
032 ing lines, providing insights to guide future model design and deployment. First,  
033 we study the scaling behavior for xLSTM in compute-optimal and over-training  
034 regimes using both IsoFLOP and parametric fit approaches on a wide range of  
035 model sizes (80M-7B) and number of training tokens (2B-2T). Second, we examine  
036 the dependence of optimal model sizes on context length, a pivotal aspect that was  
037 largely ignored in previous work. Finally, we analyze inference-time scaling char-  
038 acteristics. Our findings reveal that in typical LLM training and inference scenarios,  
039 xLSTM scales favorably compared to Transformers. Notably, xLSTM models  
040 consistently Pareto-dominate Transformer models, delivering lower cross-entropy  
041 loss for the same compute budget.  
042

## 1 INTRODUCTION

043 Scaling up models sizes and training data sets enables the recently observed rapidly advancing  
044 capabilities of Large Language Models (LLMs). As a result the computational expenses associated  
045 to training and inference of state-of-the-art LLMs results are dramatically growing. The goal of  
046 predicting the achievable performance with a specified architecture and computational resources  
047 resulted in the recent exploration in LLM scaling laws, i.e. the quantitative relationships between  
048 LLM performance metrics and the corresponding computational resources. The works of [Kaplan et al. \(2020\)](#);  
049 [Hoffmann et al. \(2022\)](#) showed that these scaling laws take the form of power laws  
050 which hold over several orders of magnitude in terms of model sizes and the number of pre-training  
051 tokens. These insights provided practical guidance in the design of recent frontier models ([Achiam et al., 2023](#);  
052 [Grattafiori et al., 2024](#); [DeepSeek-AI, 2024a](#)).

053 Recent works ([Sardana et al., 2024](#); [Gadre et al., 2024](#)) rightfully argue that these scaling laws  
054 are nevertheless limited by their neglect of inference costs. Consequently, these works focus on  
055 performance investigations on models that are trained in the so-called over-training regime, i.e. on  
056 more tokens than would be optimal in terms of pre-training compute. Importantly, these works and  
057 subsequent ones focus on Transformer architectures ([Vaswani et al., 2017](#)). In these architectures,  
058 the attention mechanism inflicts computational costs during training and inference that are *quadratic*  
059 in terms of context length. Besides the associated economic and ecological costs, this quadratic  
060 scaling is prohibitive for a large range of application areas in which models are deployed on  
061 devices with limitations on available memory, energy, or allowable TFTT. Even on GPUs that are  
062 dedicated to LLMs this scaling property of Transformers represents a limitation in task that require  
063 very long contexts, like reasoning ([Muennighoff et al., 2025](#)). Consequently, the development of  
064 LLM architectures that mitigate the attention mechanism is an active area of research ([Gu & Dao,  
065 2024](#); [Beck et al., 2024](#); [Lieber et al., 2024](#)). While these architectures were demonstrated to be  
066 scalable into the billion-parameter regime ([Zuo et al., 2024](#); [Beck et al., 2025b](#)), there is so far no  
067 systematic comparison between linear complexity LLM architectures, i.e. LLMs that scale linearly  
068 in computational costs with respect to context lengths, and transformer-based LLMs with quadratic  
069 complexity.

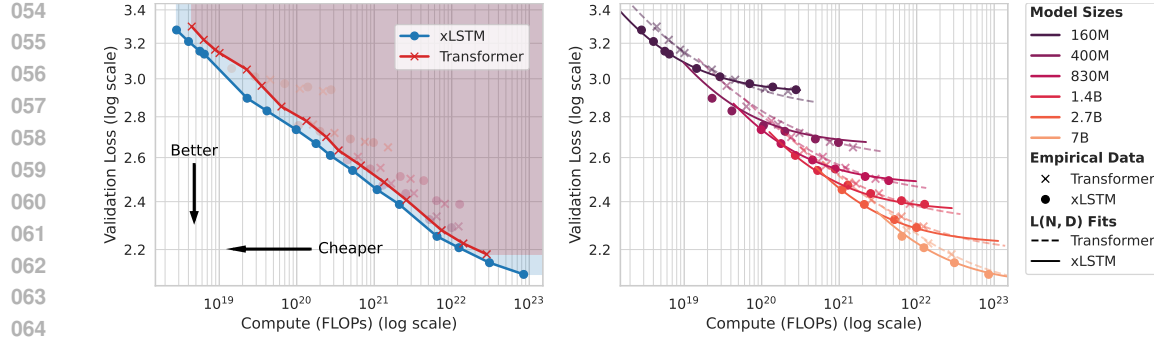


Figure 1: xLSTM scaling laws: Validation loss over training compute. **Left:** xLSTM is pareto-dominant over dense multi-head Transformers in terms of loss. For a fixed FLOP budget, xLSTM models are better. For a fixed validation loss, xLSTM models require less FLOPs. **Right:** Parametric fit of the loss surface  $L(N, D)$  as a function of model size  $N$  and dataset size  $D$ .

This work presents a systematic comparison of the scaling laws of performance-optimized xLSTM architectures (Beck et al., 2025b;a) and dense multi-head self-attention Transformer architectures (Touvron et al., 2023). Our investigations of xLSTM and Transformer models are guided by the following research questions:

- *Training*: Which architecture can be trained more efficiently in terms of computational resources and how do they scale in the practically relevant overtraining regime?
- *Context length*: How does the striking difference between xLSTM and Transformers—linear versus quadratic context length dependency—impact scaling laws and the resulting pre-training and inference performances?
- *Inference*: How does the inference speed in terms of time to first token (prefill) and step time (generation) scale for xLSTM and Transformer under different context lengths and model sizes?

Our investigation shows, that **xLSTM models Pareto-dominate Transformer models in the compute-loss trade-off** (Fig. 1), enabling models that are both better and cheaper. We find that, for a given training compute budget, compute-optimal xLSTM models are larger (Fig. 4), i.e. have more parameters, than compute-optimal Transformer models. During inference, xLSTMs are faster than same-sized Transformers (Fig. 6), and their performance advantage grows with context length due to Transformers’ quadratic time complexity.

## 2 PRELIMINARIES

We begin with a background on scaling laws and a definition of the training regimes considered in this work (Sec. 2.1). We next present approaches for scaling law fitting used in this study (Sec. 2.2).

### 2.1 BACKGROUND ON SCALING LAWS

Scaling laws for large language models predict the cross-entropy loss  $L$  as a function of the compute  $C$  used for model training in FLOPs. The compute  $C$  for training increases with larger model size measured in number of model parameters  $N$  and larger dataset size in number of training tokens  $D$ . Hence, we assume  $C$  is a function of  $N$  and  $D$ . Depending on how the total compute budget is distributed between increasing the model size and enlarging the dataset, training is typically characterized as either being in a *compute-optimal* or in an *over-training* regime.

**Compute-optimal training.** Hoffmann et al. (2022) establish the notion of compute-optimal training, which refers to the optimal choice of  $N$  and  $D$  for a given compute budget  $H$  according to the constrained optimization problem:

$$N^*(H), D^*(H) = \underset{N, D \text{ s.t. } C(N, D) = H}{\operatorname{argmin}} L(N, D). \quad (1)$$

The optimal  $N^*$  and  $D^*$  can be obtained by sweeping over  $N, D$  for each compute budget. Hoffmann et al. (2022) find that for increasing computation budgets,  $N^*$  and  $D^*$  scale roughly proportionally.

108 Assuming this proportionality, there exists a compute-optimal token per parameter ratio  $M^* = D^*/N^*$  for a fixed model class and training distribution.  
 109

110 **Over-training.** The compute-optimal allocation  $D^*, N^*$  only accounts for compute costs during  
 111 training. However, during inference larger models incur a higher inference compute cost. Taking  
 112 this into account, [Sardana et al. \(2024\)](#) argue that, once inference costs are considered, it can be  
 113 preferable to train smaller models on larger datasets. The resulting values for  $D$  and  $N$ , with a higher  
 114 than compute-optimal token per parameter ratios  $M > M^*$  is generally referred to as *over-training*  
 115 regime ([Gadre et al., 2024](#)).  
 116

117 **Calculating compute costs.** Previous works on transformer scaling laws commonly approximate  
 118 compute costs with  $C(N, D) = 6ND$  FLOPs ([Kaplan et al., 2020](#); [Hoffmann et al., 2022](#); [Gadre  
 119 et al., 2024](#); [Sardana et al., 2024](#)). This approximation ignores the FLOPs associated to the attention  
 120 mechanism and covers only the feed-forward network contributions. Recently, several works  
 121 ([DeepSeek-AI, 2024a](#); [Busbridge et al., 2025](#); [Li et al., 2025](#)) pointed out that this approximation is  
 122 not justified for sufficiently large context lengths and models. For the purpose of this work, this ap-  
 123 proximation is even less suitable since it neglects entirely the difference between linear and quadratic  
 124 time-complexity models. Hence, we adopt a more precise calculation of  $C(N, D)$  as provided in  
 125 Appendix C.3 that accurately captures the differences in computational complexity between model  
 126 classes.  
 127

## 2.2 FITTING SCALING LAWS

128 Scaling laws are obtained by fitting the dependence of the model’s training or validation loss on the  
 129 model size and the number of training tokens with power laws. Two commonly used procedures for  
 130 extracting parametric scaling laws for the loss  $L$ , depending on  $N$  and/or  $D$  are the *parametric fit*  
 131 *approach* and the *IsoFLOP approach*, which are introduced in [Hoffmann et al. \(2022\)](#) as the third  
 132 and second approach, respectively.  
 133

134 **Parametric fit approach.** Assuming that the loss  $L$  follows a power law in model parameters  $N$  and  
 135 training tokens  $D$ , the parametric fit approach estimates the observed cross-entropy loss as:  
 136

$$\hat{L}(N, D) = E + (A N^{-\alpha} + B D^{-\beta})^\gamma, \quad (2)$$

137 where  $E, A, B, \alpha, \beta$ , and  $\gamma$  are task-specific positive parameters. The constant term  $E$  accounts  
 138 for an irreducible loss component, while the second term captures the model-specific predictive  
 139 performance. While [Hoffmann et al. \(2022\)](#) set  $\gamma = 1$ , we follow the practice from [Busbridge et al.  
 140 \(2025\)](#) and treat  $\gamma$  as fit parameter.

141 A robust estimation of the scaling parameters for (2) requires data from diverse training strategies,  
 142 including non-compute optimal token-to-parameter ratios. Therefore, [Hoffmann et al. \(2022\)](#) include  
 143 data from two training strategies: (i) The number of training tokens is varied for a fixed set of models.  
 144 (ii) Model size and training tokens are both varied subject to a total compute constraint.  
 145

146 **IsoFLOP approach.** For the IsoFLOP approach a set of compute budgets  $H$  is defined and for each  
 147 budget the values of  $N$  and  $D$  are varied such that the constraint  $C(N, D) = H$  is fulfilled. Following  
 148 [Hoffmann et al. \(2022\)](#), a second-order polynomial is fitted to each of the resulting IsoFLOP profiles.  
 149 The minimum of each fit corresponds to the loss-optimal number of model parameters  $N^*(H)$  and  
 150 training tokens  $D^*(H)$  for the given compute budget  $H$ . In order to predict these quantities, we use  
 151 individual power laws of the forms  
 152

$$\hat{N}^*(H) = A' \cdot H^a \quad \text{and} \quad \hat{D}^*(H) = B' \cdot H^b, \quad (3)$$

153 where we fit the *exponents*  $a, b$  and *coefficients*  $A', B'$  from the data.  
 154

## 3 TRAINING SCALING BEHAVIOR

155 In this section, we conduct a comparative study of the scaling behavior of xLSTM and Transformer  
 156 models along multiple axes. First, we explore the pareto frontier of performance in terms of loss  
 157 and training compute in Section 3.2. Second, we study the scaling in the over-training regime with  
 158 large token to parameter ratios in Section 3.3. Finally, we determine the compute-optimal model and  
 159 dataset sizes in Section 3.4 and their dependence on the context length in Section 3.5. We begin with  
 160 the introduction of our experimental setup in Section 3.1.  
 161

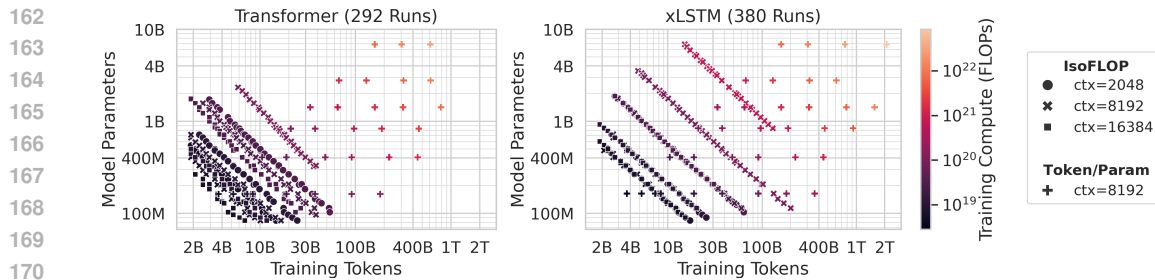


Figure 2: Dataset of training runs for our scaling law study. The dataset contains training runs for the xLSTM and the Transformer architecture, with two configurations each: *IsoFLOP* and *Token/Param*.

### 3.1 EXPERIMENTAL SETUP

To systematically study scaling behavior, we collect a large dataset of training runs across two model classes (Transformer and xLSTM) and multiple training configurations. The following describes the architectures, training recipe, and dataset of training runs used in our scaling law study.

**Model architectures: Transformer and xLSTM.** Following previous scaling law studies (Porian et al., 2024; Gadre et al., 2024), we use the dense multi-head attention decoder-only Llama-2 architecture (Touvron et al., 2023) for our Transformer models. For the xLSTM models, we consider the architecture of the recently proposed xLSTM 7B model (Beck et al., 2025b). The xLSTM-7B architecture is built entirely on mLSTM cells with parallel training mode applied within the model’s embedding dimension. Similar to the Transformer, it alternates mLSTM layers with position-wise feedforward MLP layers. The crucial distinction between the two architectures lies in the sequence-mixing mechanism: self-attention with quadratic time-complexity in Transformer versus recurrent mLSTM dynamics with linear time-complexity in xLSTM.

**Training recipe and data.** For both model classes we use the same training recipe derived from the xLSTM 7B training recipe (Beck et al., 2025b). The recipe uses the AdamW optimizer ( $\beta_1 = 0.99$ ,  $\beta_2 = 0.95$ ,  $\epsilon = 10^{-8}$ ), weight decay 0.1 and gradient clipping norm 0.5. The learning rate scheduler has three stages, linear warm-up, cosine decay to 10% of the peak learning rate, and linear cool-down. For varying compute budgets, we scale the steps in the second stage while the first and third remain fixed. Further details are given in Appendix B.1. The overall number of training steps is determined by the FLOP budget or token-to-parameter ratio of the specific experiment. As training dataset, we use DCLM-BASELINE, a collection of high-quality filtered web documents (Li et al., 2024), tokenized with the GPT-NeoX tokenizer (Black et al., 2022) into sequences of length 8192, unless specified otherwise. We use grain<sup>1</sup> to prepare batches with sequence packing, particularly first-fit packing, which avoids splitting, but adds padding tokens.

**Dataset of training runs.** Using the above defined architecture and training recipe, we produce a large dataset of training runs for our scaling law study totaling 672 individual runs (292 for Llama, 380 for xLSTM). The dataset contains model sizes ranging from 80M to 7B parameters trained with compute budgets ranging from  $2.8 \times 10^{18}$  to  $8.5 \times 10^{22}$  FLOPs on 2B to 2T tokens. This amounts to a total compute budget spent for this dataset of  $3.2 \times 10^{23}$  FLOPs. Our dataset is divided into runs from two different training configurations: *IsoFLOP* and *Token/Param*. For the IsoFLOP configuration, we vary model parameters and training tokens subject to fixed compute budgets for three different context lengths. In the Token/Param configuration, we vary the number of training tokens for a set of fixed model sizes. We show our dataset as  $\{N, D, C\}$  points in Figure 2. xLSTM’s linear scaling preserves training tokens with longer contexts (overlapping IsoFLOP points), whereas Transformer’s quadratic scaling reduces them.

### 3.2 LOSS VS. COMPUTE: xLSTM IS PARETO-DOMINANT

We begin our study with the question: Given a fixed training compute budget, which model architecture performs better (in terms of cross-entropy loss)? To answer this question, we define a grid of model and dataset sizes with pre-defined token-to-parameter ratios of

<sup>1</sup><https://google-grain.readthedocs.io> (FirstFitPackIterDataset)

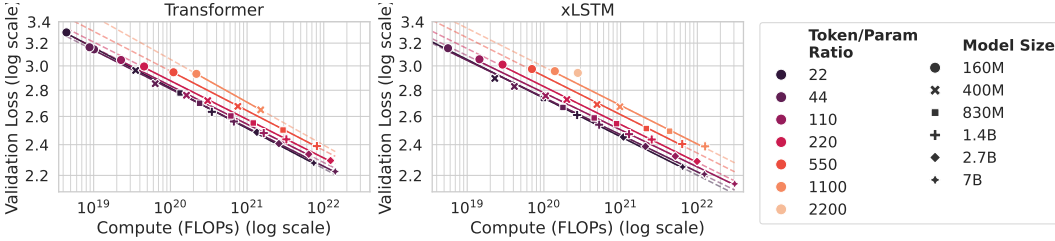


Figure 3: Power law fits to loss over training compute with increasing token-to-parameter (Token/Param) ratios  $M$ . We fit power laws of the form  $\hat{L}(C) = \lambda \cdot C^{-\eta}$  and observe that—similar to Transformer—the exponents  $\eta$  of xLSTM remain constant even for large  $M$ , indicated by the parallel lines in the log-log plot.

[22, 44, 110, 220, 550, 1100, 2200] and train Transformer and xLSTM models for each point in the grid. This forms the *Token/Param* subset in our dataset of training runs (see Sec. 3.1). We then use our FLOP calculations in Appendix C.3 and plot validation loss over FLOPs in a log-log plot in Figure 1.

**Pareto-frontier.** In Figure 1 (left), we visualize the Pareto frontier by connecting the data points for xLSTM and Transformer. We find that xLSTM is strictly dominant over Transformers across the almost five orders of magnitude of compute encompassed by our data. In other words, for a fixed FLOP budget, xLSTM models are better and for a fixed validation loss, they require less FLOPs.

**Parametric loss surface fit.** In Figure 1 (right), we fit a parametric loss surface  $\hat{L}(N, D)$  to our Token/Param data. We find that our fit of the loss surface provides a reliable description of performance of Transformer and xLSTM models for a given size even far in the over-training regime, i.e. far right to the pareto front. Following the practice of Busbridge et al. (2025), we find that including the parameter  $\gamma$  in the model of  $\hat{L}(N, D)$  improves the fit quality (see Fig. 8 in the Appendix). We provide additional details on our parametric fits in Appendix B.2.

### 3.3 xLSTM IN THE OVERTRAINING REGIME: CONSISTENT POWER LAW EXPONENTS

Our parametric  $\hat{L}(N, D)$  fit predicts, that model quality in terms of loss improves when  $N$  or  $D$  is increased. Hoffmann et al. (2022) have found that for Transformers, the optimal token-to-parameter ratio  $M^* = D^*/N^*$  that yields the minimal loss under a compute constraint is approximately 22. However, training runs with this ratio yield rather large models that are expensive and slow during inference (Sardana et al., 2024). Consequently, it is common practice to train smaller models in an overtraining regime, i.e., with token-to-parameter ratios far exceeding the compute-optimal  $M^*$ . It is thus of practical importance to demonstrate that the loss of new model architectures continues to improve with increasing amounts of data.

**Power-law exponents in over-training.** Gadre et al. (2024) have found that Transformers scale reliably in this over-training regime, indicated by constant exponents  $\eta$ , when fitting a power law of the form  $\hat{L}(C) = \lambda \cdot C^{-\eta}$  for different fixed token-per-parameter ratios  $M$ . Therefore, we perform a similar analysis and fit power laws  $\hat{L}(C)$  to our Token/Param training runs. In Figure 3 and Tab. 3 we find that—similar to Transformer—the exponents  $\eta$  of xLSTM remain constant even for large  $M$ , indicated by the parallel lines in the log-log plot. This observation is relevant because it implies that small, inference-optimized xLSTM models can be trained on large datasets while still achieving consistent improvements in loss.

### 3.4 COMPUTE-OPTIMAL xLSTM MODELS ARE LARGER

In this section, we aim to determine the compute-optimal model size  $N^*$  and dataset size  $D^*$  for the xLSTM and Transformer models. However, so far, we have performed our scaling analyses on training configurations with preset model sizes and a set of token-per-parameter ratios  $M$ , which do not allow us to determine  $N^*$  and  $D^*$  directly. Therefore, for this analysis, we use the *IsoFLOP* training configuration, where we vary the number of model parameters and training tokens subject

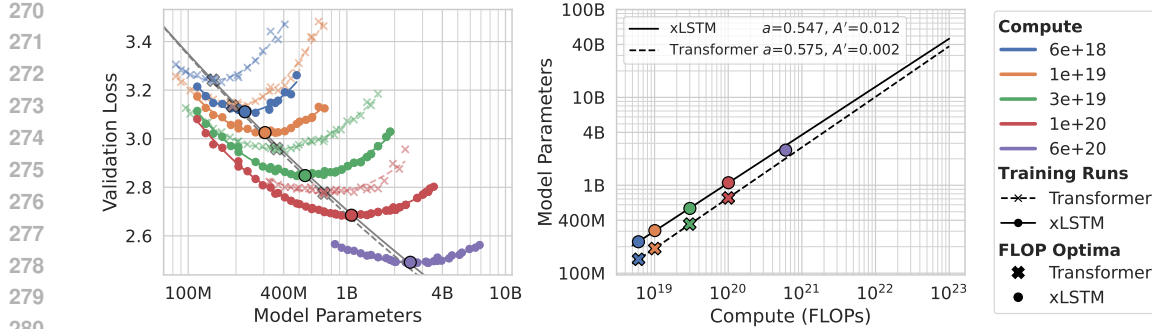


Figure 4: Varying model size and tokens with a fixed compute budget (IsoFLOP). **Left:** IsoFLOP profiles for varying number of model parameters with a marker at the minimum  $N^*$  of the fitted polynomial. **Right:** Power-law fit  $N^*(H) = A' \cdot H^a$  for the compute optimal number of model parameters. Our setup reproduces the power-law exponent  $a$  for Transformers established in Porian et al. (2024). The compute-optimal model size of xLSTMs is larger than for Transformers.

to a set of fixed compute budgets  $H$ . For each compute budget, we plot the loss over the model parameters  $N$  and number of training tokens  $D$  and fit second-order polynomials to determine the optimal  $N^*(H)$  and  $D^*(H)$  for each compute budget  $H$ . Using these optima, we then fit power laws as described in Section 2.2 to obtain the functional forms for  $\hat{N}^*(H)$  and  $\hat{D}^*(H)$  (see Eq. (3)).

**Compute-optimal model size.** In Figure 4 (left) we show the IsoFLOP profiles for variable model size and (right) the corresponding power-law fits for the optimal model size for xLSTM and Transformer. Our results show that for a given compute budget, xLSTM consistently attains a lower validation loss than Transformer, which is in line with the findings in Section 3.2. Moreover, we find that for a given compute budget, the corresponding compute-optimal xLSTM models have more parameters than the corresponding Transformer models; see Figure 4 (left and right). Note that our power-law exponent  $a$  for the Transformer matches the one found by Porian et al. (2024); see App. B.4 for details.

**Compute-optimal dataset size.** Analogous results are shown in Figure 9 in the appendix for the number of training tokens of compute-optimal models. We find that compute-optimal xLSTM and Transformer models are trained on a similar number of training tokens  $\hat{D}^*(H)$ .

**Universality of the relation between compute-optimal performance and model size.** The compute-optimal models in Figure 4 (left) fall close to a single shared line for the Transformer and xLSTM models. This suggests that for compute-optimal models, there is a universal relationship between performance and model size for xLSTM and Transformer models. From this perspective, the fact that compute-optimal xLSTM models are larger for a given compute budget can be regarded as a heuristic explanation for the superior performance of xLSTM. The reason why xLSTMs can be larger is the reduced computational complexity of their recurrent sequence-mixing operation compared to the self-attention operation in Transformers. As this main operation is cheaper, more compute can be allocated to the rest of the model, e.g. increased number of layers or embedding dimension.

### 3.5 COMPUTE-OPTIMAL xLSTM MODEL SIZE REMAINS STABLE ACROSS CONTEXT LENGTHS

The main difference between the model architectures in this study is their scaling in FLOPs with context length: Transformers scale quadratically, due to the self-attention, while xLSTMs scale linearly. This implies that, in Transformers, an increasing fraction of compute is devoted to attention as sequence length grows, whereas in xLSTMs the recurrent updates consume only a modest portion of the total compute. In this section, we investigate, therefore, the impact of the context length on compute-optimal model and dataset sizes. We add experiments with context lengths 2048 and 16384 in the IsoFLOP training configuration and then fit the power-laws to each context length for both models, analogously to Section 3.4. We note that the losses are not directly comparable across different context lengths since we use sequence packing for the construction of our training and validation datasets. Hence, for larger context lengths, longer documents can be packed into a batch, effectively changing the data distribution.

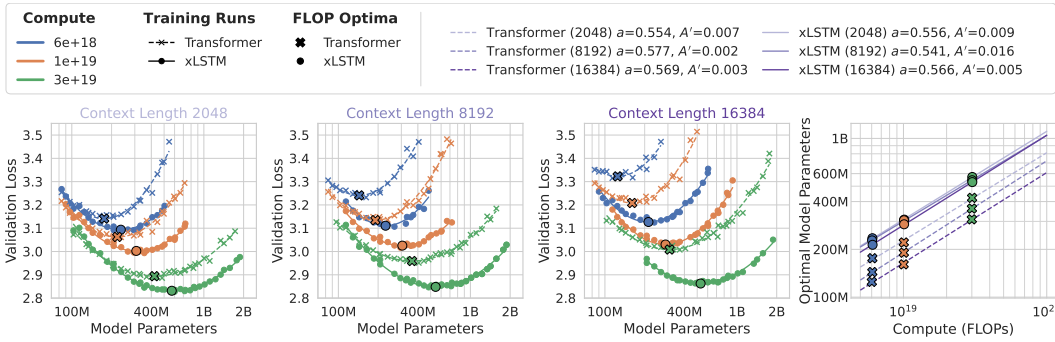


Figure 5: Left: IsoFLOP curves as a function of model parameters at 3 different context lengths. Right: Plot of the power-law fits for the compute optimal number of parameters dependent on the compute budget  $N^*(H)$ . Colors indicate compute budget and marker types indicate the model types. The compute optimal model size for Transformers gets smaller for larger context lengths, while the compute optimal model size for xLSTM remains similar across context lengths.

**Context length & compute-optimality.** In Figure 5 we show the IsoFLOP profiles for varying model sizes and three different context lengths and compute budgets, including their power-law fits  $\hat{N}^*(H)$  in the rightmost plot. We observe that with increasing context lengths the compute-optimal model size of Transformers drops significantly, while for xLSTM it drops only mildly. These results suggest that for Transformers, a growing fraction of compute is consumed by attention operations as sequence length increases, whereas in xLSTM most FLOPs remain allocated to depth and hidden dimensions. In Figure 10 in Appendix B.5 we show the corresponding IsoFLOP profiles and power-law fits  $\hat{D}^*(H)$  for the optimal number of training tokens. We observe similar trends as for the model size: The compute-optimal number of training tokens decreases markedly with larger context length for Transformer models and for xLSTM it slightly increases.

## 4 INFERENCE SCALING BEHAVIOR

The scaling laws analysis in Section 3 is motivated by the goal of the optimal design of pre-training runs for LLMs. However, these considerations neglect inference efficiency. When deploying LLMs at large scale, inference costs and performance are critical aspects. Hence Pope et al. (2023) investigate the inference efficiency of transformer-based LLMs in terms of three criteria: compute, latency, and throughput. More recently Sardana et al. (2024) provided a scaling law analysis of Transformers that extend the pre-training compute optimality consideration (Eq. (1)) to also account for inference compute. This work presents an even more comprehensive analysis in terms of the attainable latency, i.e., time to first token, and the step time during generation. We complement our empirical findings with a quantitative model of a *lower bound* on time to first token and step time, using the detailed calculation of FLOPs (App. C.3) and MemOps (App. C.4) for both model architectures.

**Inference stages.** Typically, large-scale LLM inference is split into the *prefill* and the *generation* stage (Austin et al., 2025; Pope et al., 2023; DeepSeek-AI, 2024b). In the prefill stage the LLMs process the prompt, compute the logits for the first token to be generated, and store the intermediate internal representations of the prompt, i.e. the KV cache for Transformer models or the mLSTM cell states for xLSTM. In the generation stage a token is sampled according to the logits and then the internal representations of the previous tokens in the context window are updated to account for the new token. The generation procedure is repeated for a certain budget or until the end-of-sequence token is sampled. In the following, we investigate the prefill and generation performances separately.

**Inference runtime metrics.** For the prefill stage, the key performance metric is the time to first token (TTFT). Prefill speed is primarily determined by how well the model can maintain a low TTFT while handling large batch sizes and long input sequences. During the generation stage, the key performance metric is the step time, i.e. how long it takes to obtain the next token given the current (potentially batched) sequence. For Transformers, the quadratic complexity of the attention mechanism with respect to the prefill length (App. C.3.3) implies that TTFT is expected to scale quadratically in terms of the prefill length. In terms of step time we expect linear scaling with respect

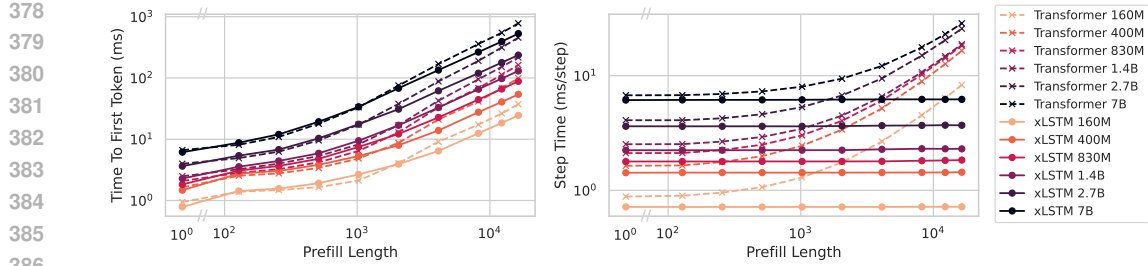


Figure 6: Scaling of TTFT (left) and step time (right) as a function of prefill length (1-16k) for different model sizes, with a batchsize of one.

to the prefill length, as each decoding step involves attention over the entire KV cache. For xLSTMs, in contrast, we expect linear scaling of TTFT and step time that is independent of the prefill length.

#### 4.1 EMPIRICAL INFERENCE RUNTIMES

We consider the same model architectures as in the *Token/Param* configuration (see Tab. 19 and 20). We utilize the implementation of xLSTM and Transformers models available through the `transformers` library (Wolf et al., 2020) and optimize runtimes using `torch.compile` and `torch.cuda.graph`. The TTFT is measured as the time needed for generating a single token under a given batch size and prefill length (i.e., the context length). The step time is measured by generating a sequence of 100 tokens, subtracting the TTFT and dividing by the sequence length. We measure the average TTFT and step time over four repetitions after two warm-up iterations.

Figure 6 presents TTFT (left) and step time (right) measurements for both architectures at matched model sizes as a function of prefill length (1-16k). At short prefills, the two model classes exhibit comparable TTFTs, while at longer prefills xLSTMs consistently achieve lower values. For 16k prefill, *xLSTM has 30-50% lower TTFT for the same model size*. This difference reflects the expected scaling: quadratically for Transformers and linearly for xLSTMs. A similar trend is observed for the step time. At small prefills, both architectures perform comparably. As the prefill length increases, the Transformer step time degrades due to the rising cost of attention over longer KV caches. In contrast, xLSTM step time is independent of prefill length, resulting in consistently higher throughput across all evaluated model sizes and prefill lengths. For 16k prefill, *the largest xLSTM has a lower step time than the smallest Transformer* we considered. In summary, when matched in model size, xLSTMs outperform Transformer models on all inference speed metrics considered.

#### 4.2 MODELING INFERENCE RUNTIMES

In our analysis, the inference processes are characterized by the associated number of floating point operations  $\text{FLOPs}_{\text{algo}}$  and the number of memory operations  $\text{Bytes}_{\text{mem,algo}}$  measured in bytes that are read or written. We provide calculations of these two quantities for xLSTM and for Transformers in Appendix C. Importantly, these calculations capture the difference between xLSTM and Transformers in the dependence of  $\text{FLOPs}_{\text{algo}}$  and  $\text{Bytes}_{\text{mem,algo}}$  on the context length  $T$ . Based on these calculated quantities, we model the runtimes associated with the floating point and memory operations as:

$$\tau_{\text{FLOPs,algo}} = \frac{\text{FLOPs}_{\text{algo}}}{\alpha_{\text{eff}}} + \epsilon, \quad \tau_{\text{mem,algo}} = \frac{\text{Bytes}_{\text{mem,algo}}}{\beta_{\text{eff}}} + \epsilon, \quad (4)$$

where  $\alpha_{\text{eff}}$  is the effective rate of  $\text{FLOPs/s}$ ,  $\beta_{\text{eff}}$  is the effective rate of  $\text{Bytes/s}$ , and  $\epsilon$  is a constant overhead when running the inference processes on the GPU. Depending on the model type, model size, prefill length, batch size and inference stage (prefill or generate), either  $\tau_{\text{FLOPs,algo}}$  or  $\tau_{\text{mem,algo}}$  is the dominant contributor to the runtime. We outline in Appendix D.1 how this is determined based on the roofline model. Using empirical runtime measurements, we then fit one of the two models depending on which one is expected to yield the dominant runtime contribution. Each fit corresponds to a specific model type, size, and inference stage, and is evaluated over varying batch sizes and prefill lengths. As evidenced by the fits to empirical TTFT (App. D.2) and step time measurements (App. D.3), our model provides an accurate description of the observed inference runtimes for both architectures and explains the empirically observed runtimes in Figure 6.

432 

## 5 RELATED WORK

433

434 **Modeling scaling behavior with parameters and data.** The empirical scaling behavior of Deep  
 435 Learning models w.r.t the size of their model parameters and training data has been actively researched  
 436 (Hestness et al., 2017; Rosenfeld et al., 2020; Henighan et al., 2020; Alabdulmohsin et al., 2022;  
 437 Caballero et al., 2023). Such scaling laws have been demonstrated across many tasks and data  
 438 modalities (Tan & Le, 2019; Ghorbani et al., 2022; Zhai et al., 2022; Abnar et al., 2022; Ardalani  
 439 et al., 2022; Gao et al., 2023) However, beginning with Kaplan et al. (2020) and Hoffmann et al.  
 440 (2022), the main objective has been guidance on how to optimally scale Large Language Models  
 441 with Transformers. Follow-up work investigated the data constrained setting (Muennighoff et al.,  
 442 2023), the effect of data pruning (Sorscher et al., 2022), extreme token per parameter ratios (Gadre  
 443 et al., 2024). Furthermore, replication efforts regarding the scaling laws established in Kaplan et al.  
 444 (2020) and Hoffmann et al. (2022) have been performed in order to reconcile their findings (Besiroglu  
 445 et al., 2024; Pearce & Song, 2024; Porian et al., 2024). Critical practical considerations such as  
 446 specific architectures and hyperparameters on the resulting scaling laws have been investigated  
 447 (McLeish et al., 2025). The recent survey Li et al. (2025) gives a comprehensive overview and  
 448 give practical guidelines in establishing scaling laws. Scaling laws have also been investigated  
 449 theoretically, providing justification for the functional forms used in practice (Amari et al., 1992;  
 450 Amari, 1993; Seung et al., 1992; Amari & Murata, 1993; Cortes et al., 1993; Yarotsky, 2018; Liang  
 451 et al., 2020; Sharma & Kaplan, 2022; Hutter, 2021; Bahri et al., 2024). For further related work on  
 452 scaling behavior beyond model parameters and training data, we refer to Appendix A.

453 **Incorporating inference characteristics into scaling laws.** Multiple studies seek to include infer-  
 454 ence characteristics such as the time-to-first-token (latency) and the time-per-token (throughput) into  
 455 their considerations on model scaling. Sardana et al. (2024) propose to incorporate inference costs  
 456 into scaling laws for an expected inference compute demand. Gadre et al. (2024) investigate scaling  
 457 laws in training regimes with high token/parameter ratios, much higher than “Chinchilla-optimal”,  
 458 which incurs higher inference speeds due to smaller models. Bian et al. (2025) devise inference-aware  
 459 scaling laws, focusing on obtaining the most inference efficient model for a certain performance.  
 460 Paliotta et al. (2025) show, that under fixed time budget during inference, distilling Transformers into  
 461 linear time-complexity Mamba models leads to higher performance on reasoning tasks, as their faster  
 462 inference speeds allow for better scaling with inference compute.

463 Closest to our work are Shen et al. (2024) and Poli et al. (2024). Shen et al. (2024) demonstrate scaling  
 464 behavior of their considered linear time-complexity architectures that is on par with Transformers.  
 465 Poli et al. (2024) shows, that hybrids between linear time-complexity and transformer models can  
 466 improve upon Transformers. Contrary, our work shows that the xLSTM linear time-complexity  
 467 architecture outscals Transformers for language modeling.

468 

## 6 LIMITATIONS AND FUTURE WORK

469

470 The main focus of this work is a comparative study of the training scaling behavior of Transformer  
 471 and xLSTM architectures in terms of cross-entropy loss. We do not consider the impact of different  
 472 training data distributions, nor do we investigate scaling behavior on other downstream tasks; instead,  
 473 we build on the findings of related work on these aspects (Sardana et al., 2024; Gadre et al., 2024;  
 474 Porian et al., 2024). Similarly, our empirical inference runtime scaling is designed to capture the  
 475 fundamental differences in computational complexity with respect to sequence length between  
 476 Transformers and xLSTM. Therefore, we adopt a fair and controlled comparative setup, focusing on  
 477 single-GPU experiments rather than exhaustive inference optimizations.

478 Future work could extend the scaling comparisons to Mixture-of-Expert or hybrid architectures  
 479 combining attention and xLSTM, explore diverse data distributions, include additional downstream  
 480 and long-context tasks, and investigate inference runtimes in production scale multi-GPU regimes to  
 481 provide further insights into efficient sequence modeling.

482 

## 7 CONCLUSION

483 Our study provides a systematic comparison of scaling behaviors between xLSTM and Transformer  
 484 architectures. We show that xLSTMs are Pareto-dominant in training loss versus compute, maintain

486 consistent power-law exponents in the overtraining regime, and scale more efficiently with context  
 487 length due to their linear complexity. While our results suggest a universal relationship between  
 488 performance and model size that applies to both compute-optimal Transformers and xLSTM models,  
 489 we find that compute-optimal xLSTM models are larger than their Transformer counterparts and that  
 490 the compute-optimal model size of xLSTMs is robust to variations in context length. During inference,  
 491 xLSTM models achieve lower time to first tokens and generation step times than Transformer models  
 492 of the same size. These results are well explained by our runtime model, which is grounded in  
 493 theoretical FLOP and memory operation calculations and shows close agreement with the empirical  
 494 data. Throughout all experiments, we find that the advantages of xLSTM grow with context length,  
 495 both for training and inference characteristics, positioning xLSTM as a promising and scalable  
 496 architecture for future language models.  
 497

## 498 REPRODUCIBILITY STATEMENT

500 We release the code to reproduce our experiments, the datasets of training runs as well as results  
 501 for inference publicly upon acceptance to facilitate future research in this direction. The datasets of  
 502 training runs have been obtained using the publicly available xLSTM 7B training repository (<https://github.com/NX-AI/xlstm-jax>) using the model configurations stated in Appendix E.  
 503 Inference results have been obtained using the publicly available benchmarking pipeline for efficient  
 504 xLSTM kernels ([https://github.com/NX-AI/mlstm\\_kernels](https://github.com/NX-AI/mlstm_kernels)), more specifically, the  
 505 model benchmarks, not those for individual kernels.  
 506

## 507 REFERENCES

509 Samira Abnar, Mostafa Dehghani, Behnam Neyshabur, and Hanie Sedghi. Exploring the Limits  
 510 of Large Scale Pre-training. In *Proceedings of the 10th International Conference on Learning  
 511 Representations (ICLR)*, 2022.

513 Samira Abnar, Harshay Shah, Dan Busbridge, Alaaeldin El-Nouby, Joshua M. Susskind, and Vimal  
 514 Thilak. Parameters vs FLOPs: Scaling laws for optimal sparsity for mixture-of-experts language  
 515 models. In *Forty-second International Conference on Machine Learning*, 2025.

516 Josh Achiam, Steven Adler, Sandhini Agarwal, Lama Ahmad, Ilge Akkaya, Florencia Leoni Aleman,  
 517 Diogo Almeida, Janko Altenschmidt, Sam Altman, Shyamal Anadkat, et al. Gpt-4 technical report.  
 518 *ArXiv*, 2303.08774, 2023.

520 Joshua Ainslie, James Lee-Thorp, Michiel de Jong, Yury Zemlyanskiy, Federico Lebron, and Sumit  
 521 Shanghai. GQA: Training Generalized Multi-Query Transformer Models from Multi-Head Check-  
 522 points. In *Proceedings of the 2023 Conference on Empirical Methods in Natural Language  
 523 Processing*, pp. 4895–4901. Association for Computational Linguistics, 2023.

524 Ibrahim M Alabdulmohsin, Behnam Neyshabur, and Xiaohua Zhai. Revisiting Neural Scaling Laws  
 525 in Language and Vision. In *Advances in Neural Information Processing Systems*, volume 35, pp.  
 526 22300–22312, 2022.

527 Shun-ichi Amari. A universal theorem on learning curves. *Neural Networks*, 6(2):161–166, 1993.  
 528 ISSN 0893-6080.

530 Shun-ichi Amari and Noboru Murata. Statistical Theory of Learning Curves under Entropic Loss  
 531 Criterion. *Neural Computation*, 5(1):140–153, 1993.

533 Shun-ichi Amari, Naotake Fujita, and Shigeru Shinomoto. Four types of learning curves. *Neural  
 534 Computation*, 4(4):605–618, 07 1992.

535 Newsha Ardalani, Carole-Jean Wu, Zeliang Chen, Bhargav Bhushanam, and Adnan Aziz. Under-  
 536 standing Scaling Laws for Recommendation Models. *ArXiv*, 2208.08489, 2022.

538 Jacob Austin, Sholto Douglas, Roy Frostig, Anselm Levskaya, Charlie Chen, Sharad Vikram, Federico  
 539 Lebron, Peter Choy, Vinay Ramasesh, Albert Webson, and Reiner Pope. How to Scale Your Model.  
*Online*, 2025. Retrieved from <https://jax-ml.github.io/scaling-book/>.

540 Yasaman Bahri, Ethan Dyer, Jared Kaplan, Jaehoon Lee, and Utkarsh Sharma. Explaining neural  
 541 scaling laws. *Proceedings of the National Academy of Sciences*, 121(27), 2024.

542

543 Maximilian Beck, Korbinian Pöppel, Markus Spanring, Andreas Auer, Oleksandra Prudnikova,  
 544 Michael Kopp, Günter Klambauer, Johannes Brandstetter, and Sepp Hochreiter. xLSTM: Extended  
 545 Long Short-Term Memory. In *Thirty-eighth Conference on Neural Information Processing Systems*,  
 546 2024.

547 Maximilian Beck, Korbinian Pöppel, Phillip Lippe, and Sepp Hochreiter. Tiled Flash Linear Attention:  
 548 More Efficient Linear RNN and xLSTM Kernels. In *The Thirty-ninth Annual Conference on  
 549 Neural Information Processing Systems*, 2025a. URL <https://openreview.net/forum?id=b6H64u6TqI>.

550

551 Maximilian Beck, Korbinian Pöppel, Phillip Lippe, Richard Kurle, Patrick M. Blies, Günter Klam-  
 552 bauer, Sebastian Böck, and Sepp Hochreiter. xLSTM 7B: A Recurrent LLM for Fast and Efficient  
 553 Inference. *ArXiv*, 2503.13427, 2025b.

554

555 Tamay Besiroglu, Ege Erdil, Matthew Barnett, and Josh You. Chinchilla Scaling: A replication  
 556 attempt. *ArXiv*, 2404.10102, 2024.

557

558 Song Bian, Minghao Yan, and Shivaram Venkataraman. Scaling Inference-Efficient Language Models.  
 559 *ArXiv*, 2501.18107, 2025.

560

561 Sid Black, Stella Biderman, Eric Hallahan, Quentin Anthony, Leo Gao, Laurence Golding, Horace He,  
 562 Connor Leahy, Kyle McDonell, Jason Phang, Michael Pieler, USVSN Sai Prashanth, Shivanshu  
 563 Purohit, Laria Reynolds, Jonathan Tow, Ben Wang, and Samuel Weinbach. GPT-NeoX-20B: An  
 564 Open-Source Autoregressive Language Model. In *Proceedings of the ACL Workshop on Challenges  
 & Perspectives in Creating Large Language Models*, 2022.

565

566 Bradley Brown, Jordan Juravsky, Ryan Ehrlich, Ronald Clark, Quoc V. Le, Christopher Ré, and  
 567 Azalia Mirhoseini. Large Language Monkeys: Scaling Inference Compute with Repeated Sampling.  
 568 *ArXiv*, 2407.21787, 2024.

569

570 Dan Busbridge, Amitis Shidani, Floris Weers, Jason Ramapuram, Eta Littwin, and Russ Webb.  
 Distillation Scaling Laws. *ArXiv*, 2502.08606, 2025.

571

572 Ethan Caballero, Kshitij Gupta, Irina Rish, and David Krueger. Broken Neural Scaling Laws. In  
 573 *Eleventh International Conference on Learning Representations (ICLR)*, 2023.

574

575 Mouxiang Chen, Binyuan Hui, Zeyu Cui, Jiaxi Yang, Dayiheng Liu, Jianling Sun, Junyang Lin, and  
 576 Zhongxin Liu. Parallel Scaling Law for Language Models. *ArXiv*, 2505.10475, 2025.

577

578 Aidan Clark, Diego De Las Casas, Aurelia Guy, Arthur Mensch, Michela Paganini, Jordan Hoffmann,  
 579 Bogdan Damoc, Blake Hechtman, Trevor Cai, Sebastian Borgeaud, George Bm Van Den Driess-  
 580 che, Eliza Rutherford, Tom Hennigan, Matthew J Johnson, Albin Cassirer, Chris Jones, Elena  
 581 Buchatskaya, David Budden, Laurent Sifre, Simon Osindero, Oriol Vinyals, Marc'Aurelio Ran-  
 582 zato, Jack Rae, Erich Elsen, Koray Kavukcuoglu, and Karen Simonyan. Unified Scaling Laws for  
 583 Routed Language Models. In Kamalika Chaudhuri, Stefanie Jegelka, Le Song, Csaba Szepesvari,  
 584 Gang Niu, and Sivan Sabato (eds.), *Proceedings of the 39th International Conference on Machine  
 Learning*, volume 162 of *Proceedings of Machine Learning Research*, pp. 4057–4086. PMLR,  
 585 17–23 Jul 2022.

586

587 Corinna Cortes, L. D. Jackel, Sara Solla, Vladimir Vapnik, and John Denker. Learning curves:  
 588 Asymptotic values and rate of convergence. In *Advances in Neural Information Processing  
 589 Systems*, volume 6, 1993.

590

591 Tri Dao. FlashAttention-2: Faster Attention with Better Parallelism and Work Partitioning. In *The  
 592 Twelfth International Conference on Learning Representations*, 2024.

593

594 DeepSeek-AI. DeepSeek-V2: A Strong, Economical, and Efficient Mixture-of-Experts Language  
 595 Model. *ArXiv*, 2405.04434, 2024a.

596

597 DeepSeek-AI. DeepSeek-V3 Technical Report. *ArXiv*, 2412.19437, 2024b.

594 Samir Yitzhak Gadre, Georgios Smyrnis, Vaishaal Shankar, Suchin Gururangan, Mitchell Wortsman,  
 595 Rulin Shao, Jean Mercat, Alex Fang, Jeffrey Li, Sedrick Keh, Rui Xin, Marianna Nezhurina, Igor  
 596 Vasiljevic, Jenia Jitsev, Alexandros G. Dimakis, Gabriel Ilharco, Shuran Song, Thomas Kollar,  
 597 Yair Carmon, Achal Dave, Reinhard Heckel, Niklas Muennighoff, and Ludwig Schmidt. Language  
 598 models scale reliably with over-training and on downstream tasks. *ArXiv*, 2403.08540, 2024.

599 Leo Gao, John Schulman, and Jacob Hilton. Scaling Laws for Reward Model Overoptimization. In  
 600 *Proceedings of the 40th International Conference on Machine Learning*, volume 202 of *Proceed-  
 601 ings of Machine Learning Research*, pp. 10835–10866. PMLR, 23–29 Jul 2023.

602 Behrooz Ghorbani, Orhan Firat, Markus Freitag, Ankur Bapna, Maxim Krikun, Xavier Garcia,  
 603 Ciprian Chelba, and Colin Cherry. Scaling Laws for Neural Machine Translation. In *Proceedings  
 604 of the 10th International Conference on Learning Representations (ICLR)*, 2022.

605 Aaron Grattafiori, Abhimanyu Dubey, Abhinav Jauhri, Abhinav Pandey, Abhishek Kadian, Ahmad  
 606 Al-Dahle, Aiesha Letman, Akhil Mathur, Alan Schelten, Alex Vaughan, and et al. The Llama 3  
 607 Herd of Models. *ArXiv*, 2407.21783, 2024.

608 Albert Gu and Tri Dao. Mamba: Linear-Time Sequence Modeling with Selective State Spaces. In  
 609 *International Conference on Learning Representations*, 2024.

610 Tom Henighan, Jared Kaplan, Mor Katz, Mark Chen, Christopher Hesse, Jacob Jackson, Heewoo  
 611 Jun, Tom B. Brown, Prafulla Dhariwal, Scott Gray, Chris Hallacy, Benjamin Mann, Alec Rad-  
 612 ford, Aditya Ramesh, Nick Ryder, Daniel M. Ziegler, John Schulman, Dario Amodei, and Sam  
 613 McCandlish. Scaling Laws for Autoregressive Generative Modeling. *ArXiv*, 2010.14701, 2020.

614 Danny Hernandez, Jared Kaplan, Tom Henighan, and Sam McCandlish. Scaling Laws for Transfer.  
 615 *ArXiv*, 2102.01293, 2021.

616 Joel Hestness, Sharan Narang, Newsha Ardalani, Gregory Diamos, Heewoo Jun, Hassan Kianinejad,  
 617 Md. Mostofa Ali Patwary, Yang Yang, and Yanqi Zhou. Deep Learning Scaling is Predictable,  
 618 Empirically. *ArXiv*, 1712.00409, 2017.

619 Jordan Hoffmann, Sebastian Borgeaud, Arthur Mensch, Elena Buchatskaya, Trevor Cai, Eliza  
 620 Rutherford, Diego de Las Casas, Lisa Anne Hendricks, Johannes Welbl, Aidan Clark, Tom  
 621 Hennigan, Eric Noland, Katie Millican, George van den Driessche, Bogdan Damoc, Aurelia Guy,  
 622 Simon Osindero, Karen Simonyan, Erich Elsen, Jack W. Rae, Oriol Vinyals, and Laurent Sifre.  
 623 Training Compute-Optimal Large Language Models. *ArXiv*, 2203.15556, 2022.

624 Marcus Hutter. Learning Curve Theory. *ArXiv*, 2102.04074, 2021.

625 Jared Kaplan, Sam McCandlish, Tom Henighan, Tom B. Brown, Benjamin Chess, Rewon Child,  
 626 Scott Gray, Alec Radford, Jeffrey Wu, and Dario Amodei. Scaling Laws for Neural Language  
 627 Models. *ArXiv*, 2001.08361, 2020.

628 Tanishq Kumar, Zachary Ankner, Benjamin F. Spector, Blake Bordelon, Niklas Muennighoff, Man-  
 629 sheej Paul, Cengiz Pehlevan, Christopher Ré, and Aditi Raghunathan. Scaling Laws for Precision.  
 630 In *Proceedings of the 13th International Conference on Learning Representations (ICLR)*, 2025.

631 Jeffrey Li, Alex Fang, Georgios Smyrnis, Maor Ivgi, Matt Jordan, Samir Gadre, Hritik Bansal, Etash  
 632 Guha, Sedrick Keh, Kushal Arora, Saurabh Garg, Rui Xin, Niklas Muennighoff, Reinhard Heckel,  
 633 Jean Mercat, Mayee Chen, Suchin Gururangan, Mitchell Wortsman, Alon Albalak, Yonatan Bitton,  
 634 Marianna Nezhurina, Amro Abbas, Cheng-Yu Hsieh, Dhruba Ghosh, Josh Gardner, Maciej Kilian,  
 635 Hanlin Zhang, Rulin Shao, Sarah Pratt, Sunny Sanyal, Gabriel Ilharco, Giannis Daras, Kalyani  
 636 Marathe, Aaron Gokaslan, Jieyu Zhang, Khyathi Chandu, Thao Nguyen, Igor Vasiljevic, Sham  
 637 Kakade, Shuran Song, Sujay Sanghavi, Fartash Faghri, Sewoong Oh, Luke Zettlemoyer, Kyle Lo,  
 638 Alaaeldin El-Nouby, Hadi Pouransari, Alexander Toshev, Stephanie Wang, Dirk Groeneveld, Luca  
 639 Soldaini, Pang Wei Koh, Jenia Jitsev, Thomas Kollar, Alexandros G. Dimakis, Yair Carmon, Achal  
 640 Dave, Ludwig Schmidt, and Vaishaal Shankar. DataComp-LM: In search of the next generation of  
 641 training sets for language models. *ArXiv*, 2406.11794, 2024.

642 Margaret Li, Sneha Kudugunta, and Luke Zettlemoyer. (Mis)Fitting: A Survey of Scaling Laws. In  
 643 *Proceedings of the International Conference on Learning Representations (ICLR)*, 2025.

648 Tengyuan Liang, Alexander Rakhlin, and Xiyu Zhai. On the Multiple Descent of Minimum-Norm  
 649 Interpolants and Restricted Lower Isometry of Kernels. In *Proceedings of Thirty Third Conference*  
 650 *on Learning Theory*, volume 125, pp. 2683–2711. PMLR, 2020.

651 Opher Lieber, Barak Lenz, Hofit Bata, Gal Cohen, Jhonathan Osin, Itay Dalmedigos, Erez Safahi,  
 652 Shaked Meirom, Yonatan Belinkov, Shai Shalev-Shwartz, Omri Abend, Raz Alon, Tomer Asida,  
 653 Amir Bergman, Roman Glzman, Michael Gokhman, Avashalom Manevich, Nir Ratner, Noam  
 654 Rozen, Erez Shwartz, Mor Zusman, and Yoav Shoham. Jamba: A Hybrid Transformer-Mamba  
 655 Language Model. *ArXiv*, 2403.19887, 2024.

656 Sean McLeish, John Kirchenbauer, David Yu Miller, Siddharth Singh, Abhinav Bhatele, Micah  
 657 Goldblum, Ashwinee Panda, and Tom Goldstein. Gemstones: A Model Suite for Multi-Faceted  
 658 Scaling Laws. *ArXiv*, 2502.06857, 2025.

659 Niklas Muennighoff, Alexander Rush, Boaz Barak, Teven Le Scao, Nouamane Tazi, Aleksandra  
 660 Piktus, Sampo Pyysalo, Thomas Wolf, and Colin A Raffel. Scaling Data-Constrained Language  
 661 Models. In *Advances in Neural Information Processing Systems*, volume 36, pp. 50358–50376,  
 662 2023.

663 Niklas Muennighoff, Zitong Yang, Weijia Shi, Xiang Lisa Li, Li Fei-Fei, Hannaneh Hajishirzi, Luke  
 664 Zettlemoyer, Percy Liang, Emmanuel Candès, and Tatsunori Hashimoto. s1: Simple test-time  
 665 scaling. *ArXiv*, 2501.19393, 2025.

666 OpenAI. Learning to reason with LLMs, 2024. URL <https://openai.com/index/learning-to-reason-with-l1lms/>. Accessed: 2025/05/23.

667 Daniele Paliotta, Junxiong Wang, Matteo Pagliardini, Kevin Y. Li, Aviv Bick, J. Zico Kolter, Albert  
 668 Gu, François Fleuret, and Tri Dao. Thinking Slow, Fast: Scaling Inference Compute with Distilled  
 669 Reasoners. *ArXiv*, 2502.20339, 2025.

670 Tim Pearce and Jinyeop Song. Reconciling Kaplan and Chinchilla Scaling Laws. *Transactions on  
 671 Machine Learning Research*, 2024.

672 Michael Poli, Armin W Thomas, Eric Nguyen, Pragaash Ponnusamy, Björn Deisereth, Kristian  
 673 Kersting, Taiji Suzuki, Brian Hie, Stefano Ermon, Christopher Ré, Ce Zhang, and Stefano Massaroli.  
 674 Mechanistic Design and Scaling of Hybrid Architectures. *ArXiv*, 2403.17844, 2024.

675 Reiner Pope, Sholto Douglas, Aakanksha Chowdhery, Jacob Devlin, James Bradbury, Anselm  
 676 Levskaya, Jonathan Heek, Kefan Xiao, Shivani Agrawal, and Jeff Dean. Efficiently Scaling  
 677 Transformer Inference. In *Proceedings of the 6th Conference on Machine Learning and Systems  
 (MLSys)*, 2023.

678 Tomer Porian, Mitchell Wortsman, Jenia Jitsev, Ludwig Schmidt, and Yair Carmon. Resolving Dis-  
 679 crepancies in Compute-Optimal Scaling of Language Models. In *Advances in Neural Information  
 680 Processing Systems*, volume 37, pp. 100535–100570, 2024.

681 Jonathan S. Rosenfeld, Amir Rosenfeld, Yonatan Belinkov, and Nir Shavit. A Constructive Pre-  
 682 diction of the Generalization Error Across Scales. In *International Conference on Learning  
 683 Representations*, 2020.

684 Nikhil Sardana, Jacob Portes, Sasha Doubov, and Jonathan Frankle. Beyond Chinchilla-optimal:  
 685 accounting for inference in language model scaling laws. In *International Conference on Machine  
 686 Learning (ICML)*, 2024.

687 H. S. Seung, H. Sompolinsky, and N. Tishby. Statistical mechanics of learning from examples. *Phys.  
 688 Rev. A*, 45:6056–6091, Apr 1992.

689 Utkarsh Sharma and Jared Kaplan. Scaling Laws from the Data Manifold Dimension. *Journal of  
 690 Machine Learning Research*, 23(9):1–34, 2022.

691 Noam Shazeer, Azalia Mirhoseini, Krzysztof Maziarz, Andy Davis, Quoc Le, Geoffrey Hinton, and  
 692 Jeff Dean. Outrageously Large Neural Networks: The Sparsely-Gated Mixture-of-Experts Layer.  
 693 In *Proceedings of the 5th International Conference on Learning Representations (ICLR)*, 2017.

702 Xuyang Shen, Dong Li, Ruitao Leng, Zhen Qin, Weigao Sun, and Yiran Zhong. Scaling Laws for  
 703 Linear Complexity Language Models. *ArXiv*, 2406.16690, 2024.

704

705 Jingzhe Shi, Qinwei Ma, Hongyi Liu, Hang Zhao, Jeng-Neng Hwang, and Lei Li. Explaining Context  
 706 Length Scaling and Bounds for Language Models. *ArXiv*, 2502.01481, 2025.

707

708 Charlie Snell, Jaehoon Lee, Kelvin Xu, and Aviral Kumar. Scaling LLM Test-Time Compute  
 709 Optimally Can Be More Effective than Scaling Parameters for Reasoning. In *Proceedings of the*  
 710 *13th International Conference on Learning Representations (ICLR)*, 2025.

711

712 Ben Sorscher, Robert Geirhos, Shashank Shekhar, Surya Ganguli, and Ari Morcos. Beyond neural  
 713 scaling laws: beating power law scaling via data pruning. In *Advances in Neural Information*  
 714 *Processing Systems*, volume 35, pp. 19523–19536, 2022.

715

716 Jacob Mitchell Springer, Sachin Goyal, Kaiyue Wen, Tanishq Kumar, Xiang Yue, Sadhika Malladi,  
 717 Graham Neubig, and Aditi Raghunathan. Overtrained language models are harder to fine-tune. In  
 718 *Forty-second International Conference on Machine Learning*, 2025.

719

720 Mingxing Tan and Quoc Le. EfficientNet: Rethinking Model Scaling for Convolutional Neural  
 721 Networks. In Kamalika Chaudhuri and Ruslan Salakhutdinov (eds.), *Proceedings of the 36th*  
 722 *International Conference on Machine Learning*, volume 97 of *Proceedings of Machine Learning*  
 723 *Research*, pp. 6105–6114. PMLR, 09–15 Jun 2019.

724

725 Chaofan Tao, Qian Liu, Longxu Dou, Niklas Muennighoff, Zhongwei Wan, Ping Luo, Min Lin, and  
 726 Ngai Wong. Scaling Laws with Vocabulary: Larger Models Deserve Larger Vocabularies. In  
 727 *Advances in Neural Information Processing Systems*, volume 37, pp. 114147–114179, 2024.

728

729 Hugo Touvron, Louis Martin, Kevin Stone, Peter Albert, Amjad Almahairi, Yasmine Babaei, Nikolay  
 730 Bashlykov, Soumya Batra, Prajjwal Bhargava, Shruti Bhosale, Dan Bikel, Lukas Blecher, Cris-  
 731 tian Canton Ferrer, Moya Chen, Guillem Cucurull, David Esiobu, Jude Fernandes, Jeremy Fu,  
 732 Wenyin Fu, Brian Fuller, Cynthia Gao, Vedanuj Goswami, Naman Goyal, Anthony Hartshorn,  
 733 Saghar Hosseini, Rui Hou, Hakan Inan, Marcin Kardas, Viktor Kerkez, Madian Khabsa, Isabel  
 734 Kloumann, Artem Korenev, Punit Singh Koura, Marie-Anne Lachaux, Thibaut Lavril, Jenya Lee,  
 735 Diana Liskovich, Yinghai Lu, Yuning Mao, Xavier Martinet, Todor Mihaylov, Pushkar Mishra,  
 736 Igor Molybog, Yixin Nie, Andrew Poulton, Jeremy Reizenstein, Rashi Rungta, Kalyan Saladi,  
 737 Alan Schelten, Ruan Silva, Eric Michael Smith, Ranjan Subramanian, Xiaoqing Ellen Tan, Binh  
 738 Tang, Ross Taylor, Adina Williams, Jian Xiang Kuan, Puxin Xu, Zheng Yan, Iliyan Zarov, Yuchen  
 739 Zhang, Angela Fan, Melanie Kambadur, Sharan Narang, Aurelien Rodriguez, Robert Stojnic,  
 740 Sergey Edunov, and Thomas Scialom. Llama 2: Open Foundation and Fine-Tuned Chat Models.  
 741 *ArXiv*, 2307.09288, 2023.

742

743 Ashish Vaswani, Noam Shazeer, Niki Parmar, Jakob Uszkoreit, Llion Jones, Aidan N Gomez, Łukasz  
 744 Kaiser, and Illia Polosukhin. Attention is All you Need. In *Advances in Neural Information*  
 745 *Processing Systems*, volume 30, 2017.

746

747 Samuel Williams, Andrew Waterman, and David Patterson. Roofline: an insightful visual performance  
 748 model for multicore architectures. *Commun. ACM*, 52(4):65–76, 2009.

749

750 Thomas Wolf, Lysandre Debut, Victor Sanh, Julien Chaumond, Clement Delangue, Anthony Moi,  
 751 Pierrick Cistac, Tim Rault, Rémi Louf, Morgan Funtowicz, Joe Davison, Sam Shleifer, Patrick  
 752 von Platen, Clara Ma, Yacine Jernite, Julien Plu, Canwen Xu, Teven Le Scao, Sylvain Gugger,  
 753 Mariama Drame, Quentin Lhoest, and Alexander M. Rush. Transformers: State-of-the-art natural  
 754 language processing. In *Proceedings of the 2020 Conference on Empirical Methods in Natural*  
 755 *Language Processing: System Demonstrations*. Association for Computational Linguistics, 2020.

756

757 Wenhao Xiong, Jingyu Liu, Igor Molybog, Hejia Zhang, Prajjwal Bhargava, Rui Hou, Louis Martin,  
 758 Rashi Rungta, Karthik Abinav Sankararaman, Barlas Oguz, Madian Khabsa, Han Fang, Yashar  
 759 Mehdad, Sharan Narang, Kshitiz Malik, Angela Fan, Shruti Bhosale, Sergey Edunov, Mike Lewis,  
 760 Sinong Wang, and Hao Ma. Effective Long-Context Scaling of Foundation Models. In *Proceedings*  
 761 *of the 2024 Conference of the North American Chapter of the Association for Computational*  
 762 *Linguistics: Human Language Technologies (Volume 1: Long Papers)*, pp. 4643–4663, 2024.

756 Dmitry Yarotsky. Optimal approximation of continuous functions by very deep ReLU networks. In  
757 *Proceedings of the 31st Conference On Learning Theory*, volume 75, pp. 639–649. PMLR, 2018.  
758

759 Xiaohua Zhai, Alexander Kolesnikov, Neil Houlsby, and Lucas Beyer. Scaling Vision Transformers.  
760 In *Proceedings of the IEEE/CVF Conference on Computer Vision and Pattern Recognition (CVPR)*,  
761 pp. 12104–12113, June 2022.

762 Rosie Zhao, Tian Qin, David Alvarez-Melis, Sham Kakade, and Naomi Saphra. Distributional  
763 Scaling Laws for Emergent Capabilities. *ArXiv*, 2502.17356, 2025.

764

765 Jingwei Zuo, Maksim Velikanov, Dhia Eddine Rhaiem, Ilyas Chahed, Younes Belkada, Guillaume  
766 Kunsch, and Hakim Hacid. Falcon Mamba: The First Competitive Attention-free 7B Language  
767 Model. *ArXiv*, 2410.05355, 2024.

768

769

770

771

772

773

774

775

776

777

778

779

780

781

782

783

784

785

786

787

788

789

790

791

792

793

794

795

796

797

798

799

800

801

802

803

804

805

806

807

808

809

810	APPENDIX	
811		
812	CONTENTS	
813		
814		
815	<b>1</b> <b>Introduction</b>	<b>1</b>
816		
817	<b>2</b> <b>Preliminaries</b>	<b>2</b>
818	2.1 Background on Scaling Laws . . . . .	2
819	2.2 Fitting Scaling Laws . . . . .	3
820		
821		
822	<b>3</b> <b>Training Scaling Behavior</b>	<b>3</b>
823	3.1 Experimental Setup . . . . .	4
824	3.2 Loss vs. Compute: xLSTM is Pareto-Dominant . . . . .	4
825	3.3 xLSTM in the Overtraining Regime: Consistent Power Law Exponents . . . . .	5
826	3.4 Compute-Optimal xLSTM Models are Larger . . . . .	5
827	3.5 Compute-optimal xLSTM model size remains stable across Context Lengths . . . . .	6
828		
829		
830		
831	<b>4</b> <b>Inference Scaling Behavior</b>	<b>7</b>
832	4.1 Empirical Inference Runtimes . . . . .	8
833	4.2 Modeling Inference Runtimes . . . . .	8
834		
835		
836	<b>5</b> <b>Related Work</b>	<b>9</b>
837		
838		
839	<b>6</b> <b>Limitations and Future Work</b>	<b>9</b>
840		
841	<b>7</b> <b>Conclusion</b>	<b>9</b>
842		
843	<b>A</b> <b>Extended Related Work</b>	<b>18</b>
844		
845		
846	<b>B</b> <b>Extended Training Scaling Behavior</b>	<b>18</b>
847	B.1 Details on the Experimental Setup . . . . .	18
848	B.2 Details on the Parametric Loss Surface Fit . . . . .	19
849	B.3 Power-Law Exponents in Over-Training . . . . .	20
850	B.4 Additional Results: IsoFLOP Approach . . . . .	20
851	B.5 Additional Results: IsoFLOP Approach for Different Context Lengths . . . . .	21
852		
853		
854		
855	<b>C</b> <b>Accounting: Parameters, Cache Sizes, FLOPs, Memory Operations</b>	<b>23</b>
856		
857	C.1 Parameter Counts . . . . .	24
858	C.1.1 mLSTM Params . . . . .	24
859	C.1.2 Transformer Params . . . . .	24
860	C.2 Memory State and KV-Cache Size . . . . .	24
861	C.3 FLOP Counts . . . . .	25
862	C.3.1 mLSTM Cell FLOPs . . . . .	25
863		

---

864	C.3.2 mLSTM Model FLOPs . . . . .	26
865	C.3.3 Self-Attention FLOPs . . . . .	27
866	C.3.4 Transformer Model FLOPs . . . . .	28
867		
868	<b>C.4 Memory Operation Counts . . . . .</b>	<b>29</b>
869	C.4.1 mLSTM Cell MemOps . . . . .	29
870	C.4.2 mLSTM Model MemOps . . . . .	29
871	C.4.3 Self-Attention MemOps . . . . .	30
872		
873	C.4.4 Transformer Model MemOps . . . . .	31
874		
875		
876		
877	<b>D Modeling Inference Characteristics . . . . .</b>	<b>32</b>
878	D.1 Background: Theoretical Runtime . . . . .	32
879	D.2 Prefill Stage: Time To First Token . . . . .	33
880		
881	D.3 Generation Stage: Step Time . . . . .	34
882		
883	<b>E Model Configurations . . . . .</b>	<b>36</b>
884	E.1 Model Sizes and Hyperparameters in Token/Param Configuration . . . . .	36
885		
886	E.2 Model Sizes and Hyperparameters in IsoFLOP Configuration . . . . .	37
887		
888		
889		
890		
891		
892		
893		
894		
895		
896		
897		
898		
899		
900		
901		
902		
903		
904		
905		
906		
907		
908		
909		
910		
911		
912		
913		
914		
915		
916		
917		

918 A EXTENDED RELATED WORK  
919  
920

921 **Other scaling behaviors.** Beyond scaling behavior with model parameters and training data, other  
922 scaling behaviors have been investigated. Hernandez et al. (2021) considers scaling laws for transfer  
923 learning. Clark et al. (2022) and Abnar et al. (2025) investigate scaling laws for routed language  
924 models, such as the widely considered Mixture-of-Experts method (Shazeer et al., 2017). Scaling  
925 inference compute is a major consideration for LLM reasoning models (OpenAI, 2024). For example  
926 Snell et al. (2025); Brown et al. (2024); Muenninghoff et al. (2025) demonstrated such scaling  
927 behavior with additional inference tokens. Kumar et al. (2025) devise precision-aware scaling laws,  
928 investigating the tradeoffs between precision, parameters and data. Tao et al. (2024) suggest the  
929 vocabulary size as additional parameter when scaling language models. Busbridge et al. (2025)  
930 investigate scaling laws for distilled models based on the compute budget allocation between teacher  
931 and student. Zhao et al. (2025) reconcile the smooth improvements predicted by scaling laws with  
932 the reported sudden emergent capabilities of LLMs at scale through distributional scaling laws. Chen  
933 et al. (2025) introduce parallel scaling laws, where compute is scaled by using a single set of model  
934 parameters in parallel with different learnable input transformations and output aggregation. Related  
935 to our work, Xiong et al. (2024) and Shi et al. (2025) investigate the scaling behavior of transformer  
936 models w.r.t. their context length. Springer et al. (2025) show that overtrained models are harder to  
937 fine-tune.

938  
939 B EXTENDED TRAINING SCALING BEHAVIOR  
940  
941942 B.1 DETAILS ON THE EXPERIMENTAL SETUP  
943  
944

945 We provide additional details on our experiments, that we conducted on a cluster of NVIDIA H100  
946 GPUs.

947 **Model Configurations.** In Appendix E we provide a list of model architecture configurations for  
948 all Transformer and xLSTM models used in our scaling law study in Token/Param (App. E.1) and  
949 IsoFLOP (App. E.2) training setups.

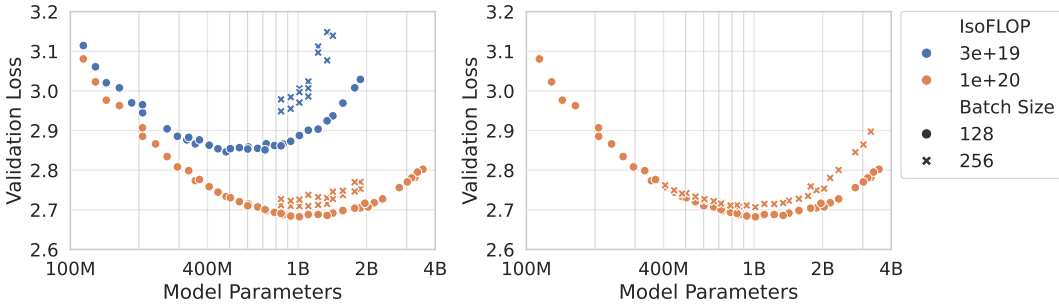
950 **General Hyperparameters.** We use the AdamW optimizer with  $\beta_1 = 0.99$ ,  $\beta_2 = 0.95$ ,  $\epsilon = 10^{-8}$ ,  
951 weight decay 0.1 and gradient clipping norm 0.5. Our learning rate schedule comprises three stages:  
952 A linear warm-up of 750 training steps, a cosine decay to 10% of the peak learning rate and a  
953 final linear cool-down of 1000 training steps. While we keep the steps for warm-up and cool-down  
954 constant, we match length of our learning rate decay to the token budget, which is either determined  
955 by a specific token-to-parameter ratio or a compute budget for a given model size (see Sec. 3.1).  
956 Unless specified otherwise, we use a context length of 8192 for our scaling law study.

957 **Hyperparameters for Token/Param setup.** We specify our batch sizes and learning rates for  
958 our experiments in the overtraining regime with large token-to-parameter ratios for xLSTM and  
959 Transformer models in Tab. 19 and 20, respectively. For larger models we decrease the learning rate  
960 and use larger batch sizes. We find that for very large token-to-parameter ratios the performance in  
961 terms of validation loss becomes less sensitive to the choice of learning rate.

962 **Hyperparameters for IsoFLOP setup.** For our IsoFLOP experiments we use a batch size of 1M  
963 tokens for all but the largest compute budget of 6e+20 FLOPs, where we double the batch size to  
964 2M tokens, as the training runs would become prohibitively long (see Tab. 1). In contrast to the  
965 Token/Param experiments, we do not increase the batch size with model size, since we found that this  
966 leads to loss offsets in the isoflop profiles (see Fig. 7, left). Instead, we keep the batch size constant  
967 for each compute budget, regardless of the model size. We validate this choice by repeating the  
968 experiments for the isoflop profile with compute budget 1e+20 with a batch size of 1M and 2M tokens.  
969 We find that the larger batch size yields a higher validation loss due to fewer training steps, but does  
970 not have a major impact on the optimal number of parameters  $N^*$  for this compute budget (see Fig. 7,  
971 right). Starting from the Token/Param learning rates, we tune the learning rates for selected model  
972 sizes, and use the best learning rates for models of similar size.

972 Table 1: Batch sizes used for the IsoFLOP training setup at context length  $T = 8192$ . For the other  
 973 context lengths  $T$  we adjust  $B$  such that batch size in number of tokens  $B \times T$  remains constant.  
 974

IsoFLOP	$B$ (seqs)	$B \times T$ (tokens)
6e+18	128	1,048,576
1e+19	128	1,048,576
3e+19	128	1,048,576
1e+20	128	1,048,576
6e+20	256	2,097,152



993 Figure 7: Impact of the batch size on IsoFLOP profiles. **Left:** IsoFLOP curves with large batch size  
 994 and different learning rates for large models. Varying the batch size for different model sizes, leads  
 995 to offsets in the IsoFLOP profile, which are more pronounced for smaller compute budgets. **Right:**  
 996 IsoFLOP profile for compute budget  $1e+20$  with different batch sizes. The larger batch size leads to  
 997 larger loss, but similar optimal model size.

## 1000 B.2 DETAILS ON THE PARAMETRIC LOSS SURFACE FIT

1001 For the parametric loss surface fit  $\hat{L}(N, D)$  in Figure 1 we follow the procedure outlined in [Bus-](#)  
 1002 [bridge et al. \(2025, App. F.1\)](#). We fit the coefficients  $\{E, A, B, \alpha, \beta, \gamma\}$  for the parametric func-  
 1003 tion of the loss surface  $\hat{L}(N, D)$  in (2) with different values for the Huber  $\delta$ . Similar to [Bus-](#)  
 1004 [bridge et al. \(2025\)](#), we observe that including  $\gamma$ , significantly improves the quality of our fits  
 1005 (see Fig. 8). We use the Token/Param training configurations for Transformer (31 samples)  
 1006 and xLSTM (35 samples) from our dataset of training runs and fit over a grid of L-BFGS-B  
 1007 initializations given by:  $\log A \in \{0.0, 5.0, 10.0, 15.0, 20.0\}$ ,  $\log B \in \{0.0, 5.0, 10.0, 15.0, 20.0\}$ ,  
 1008  $\log E \in \{-1.0, -0.5, 0.0, 0.5, 1.0\}$ ,  $\alpha \in \{0.0, 0.2, 0.5, 1.0\}$ ,  $\beta \in \{0.0, 0.2, 0.5, 1.0\}$  and  $\gamma \in$   
 1009  $\{0.0, 0.5, 1.0, 1.5\}$ .

1010 In Tab. 2, we report the coefficients that achieve the lowest MSE on the fit data out of all initializations  
 1011 for different Huber  $\delta$ . We find that the optimal fit parameters are sensitive to the choice of  $\delta$ . For  
 1012  $\delta \geq 0.1$  the optimal values for the fit parameters did not change in the digits shown in Tab. 2.

1015 Table 2: Optimal fit parameters for the loss surface  $\hat{L}(N, D)$  model from equation (2) for Transformer  
 1016 and xLSTM models for different Huber  $\delta$ . In Figure 1 we plot the fit for  $\delta = 10^{-3}$ .

	Huber $\delta$	$\log A$	$\log B$	$\log E$	$\alpha$	$\beta$	$\gamma$
Transformer	$10^{-5}$	12.96	14.35	0.05	0.58	0.55	0.28
	$10^{-3}$	11.99	13.35	0.01	0.53	0.51	0.29
	$\geq 10^{-1}$	14.45	16.33	0.09	0.64	0.63	0.25
xLSTM	$10^{-5}$	16.13	17.10	0.07	0.71	0.66	0.24
	$10^{-3}$	16.22	17.31	0.11	0.73	0.67	0.24
	$\geq 10^{-1}$	15.46	16.53	0.18	0.71	0.65	0.26

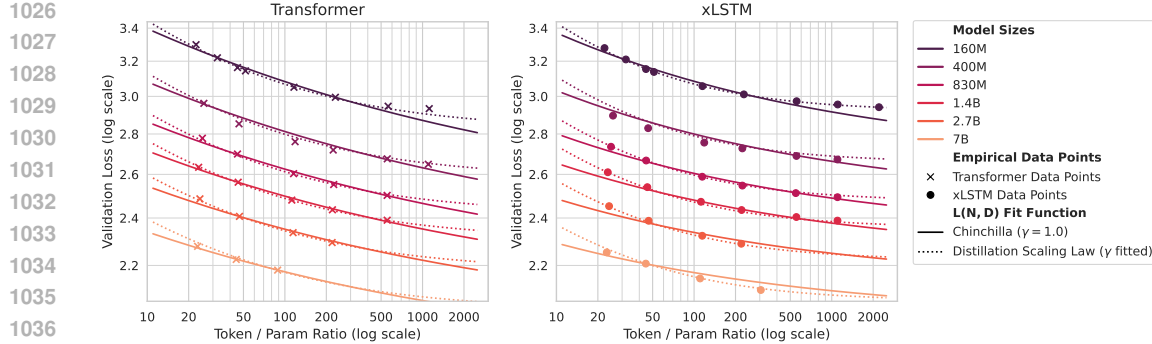


Figure 8: Comparison between the parametric fit with  $\gamma = 1$  (Hoffmann et al., 2022) and  $\gamma$  as free parameter (Busbridge et al., 2025). Including  $\gamma$  as fit parameter improves the fit quality.

### B.3 POWER-LAW EXPONENTS IN OVER-TRAINING

In Tab. 3 we report the power-law exponents for different token-to-parameter ratios  $M$ .

Table 3: Power-law exponents  $\eta$  for increasing token-to-parameter ratios  $M$ .

$M$	Transformer	xLSTM
22	0.050	0.047
44	0.048	0.046
110	0.047	0.046
220	0.048	0.047
550	0.049	0.047
1100	-	0.047

### B.4 ADDITIONAL RESULTS: ISOFLOP APPROACH

**Comparison of our scaling law to Porian et al. (2024).** In order to validate our scaling law framework, we compare our power-law fits for the optimal model size from Fig. 4 with the results from Porian et al. (2024). Porian et al. (2024) investigate and resolve the discrepancies in scaling laws between the influential works by Kaplan et al. (2020) and Hoffmann et al. (2022). We find that our power-law coefficient  $a_{\text{ours}} = 0.575$  is very close to the coefficient reported in Figure 1d) from Porian et al. (2024) with  $a_{\text{Porian,d}} = 0.571$  and even falls well into their confidence interval of  $(0.56, 0.59)$ , despite the well-documented reproducibility challenges in scaling laws (Porian et al., 2024; Li et al., 2025; McLeish et al., 2025). Porian et al. (2024) report that for their  $a_{\text{Porian,d}}$  they match their learning rate cosine decay schedule to each token budget – a practice that we follow in our experimental setup (see App. B.1). This agreement validates our framework and affirms its credibility. As the final step, to fully match the coefficients reported by Hoffmann et al. (2022), Porian et al. (2024) report that it is necessary to tune learning rate, batch size and AdamW  $\beta_2$  parameter individually for each model size. However, in our case this would require considerably more compute resources due to our much larger compute budgets ( $6e+18 - 6e+20$ ), and hence larger model sizes used for our scaling law study.

**Compute-optimal dataset size.** In the main paper (Sec. 3.4, Fig 4), we presented results for the compute-optimal model size. In Fig. 9 we present results w.r.t. the number of training tokens. We observe that compute-optimal xLSTMs and Transformers are trained on a similar number of tokens.

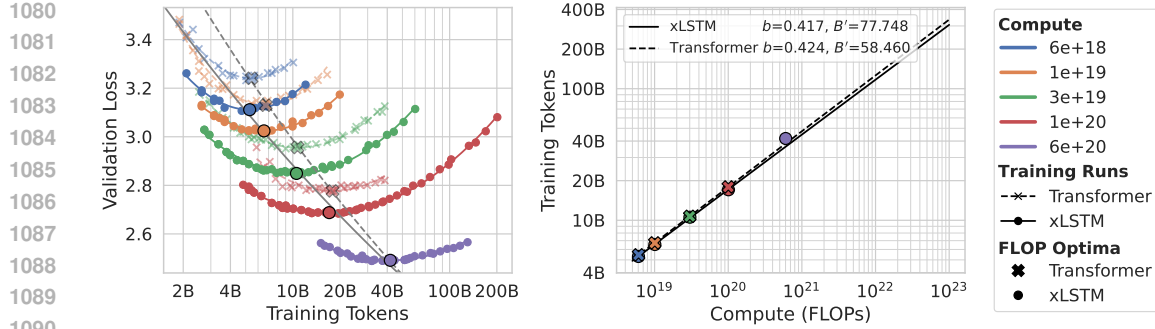


Figure 9: Left: IsoFLOP curves for varying number of training tokens with a marker at the minimum of the fit. Right: Plot of the power-law fit for the compute optimal number of training tokens  $D^*(C)$ . Colors indicate compute budget and marker types indicate the model types.

## B.5 ADDITIONAL RESULTS: ISOFLOP APPROACH FOR DIFFERENT CONTEXT LENGTHS

Complementary to the IsoFLOP results in Sec 3.5, where we showed scaling behavior w.r.t. the model parameters, we also show the scaling behavior w.r.t. the dataset size. The results are provided in Figure 10, showing that for xLSTM it slightly increases with context length, whereas for Transformer it substantially decreases. This is caused by the quadratic cost of the attention mechanism that becomes dominant at larger context lengths, causing substantial compute that shifts compute-optimal models towards smaller models that are trained on less tokens. For all considered context lengths, it is favorable to train an xLSTM model compared to a Transformer model under the same compute budget. The longer the training context length, the more favorable it is to train an xLSTM compared to a Transformer.

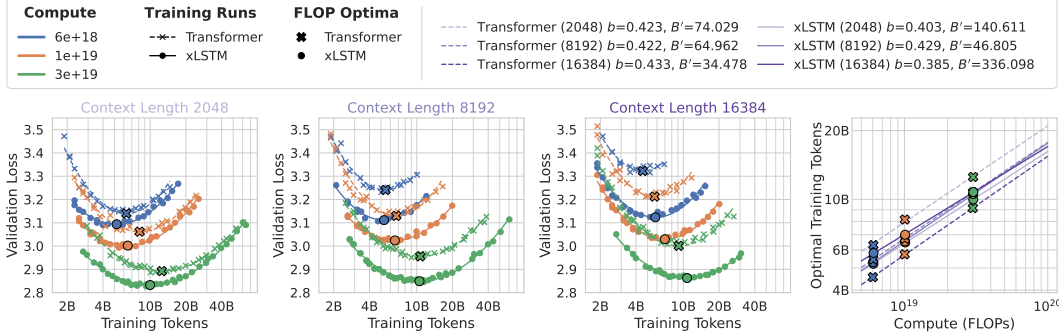
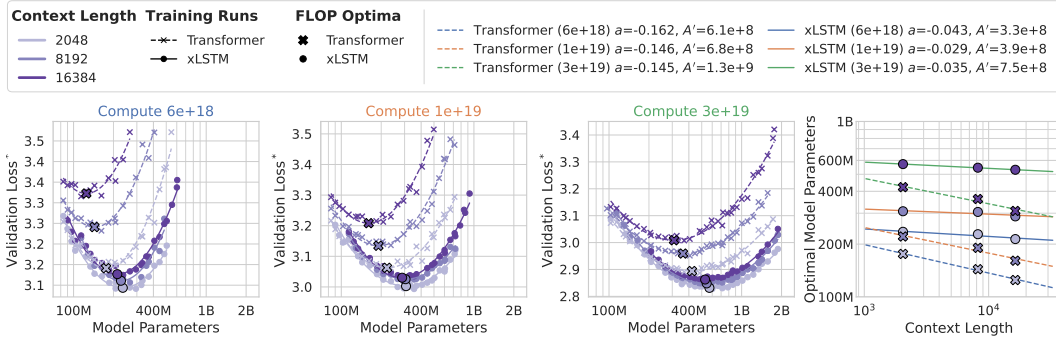


Figure 10: IsoFLOP curves for xLSTM and Transformer for different context lengths and varying number of training tokens.

By rearranging the data obtained from the IsoFLOP approach under different context lengths, one can also fit scaling laws for the context length. This is done equivalently to scaling laws for the model parameters and number of training tokens (Eq. (3)). Figure 11 shows the results w.r.t. the number of model parameters and Figure 12 shows the results w.r.t. the number of training tokens. The obtained scaling laws mirror the findings from before. Compute-optimal xLSTM models have more or less constant model size and use slightly more tokens w.r.t. the context length. Compute-optimal Transformer models are becoming smaller and use less training tokens w.r.t. the context length.

1134  
1135  
1136  
1137  
1138  
1139



1140  
1141  
1142  
1143  
1144  
1145  
1146  
1147  
1148  
1149  
1150  
1151  
1152  
1153  
1154  
1155  
1156  
1157  
1158  
1159  
1160  
1161  
1162  
1163  
1164  
1165  
1166  
1167  
1168  
1169  
1170  
1171  
1172  
1173  
1174  
1175  
1176  
1177  
1178  
1179  
1180  
1181  
1182  
1183  
1184  
1185  
1186  
1187

Figure 11: Left: IsoFLOP curves for xLSTM and Llama as a function of model parameters at 3 different compute budgets. Right: Plot of the power-law fits for the compute optimal number of parameters dependent on the context length  $N^*(T)$ . Colors indicate context length and marker types indicate the model types.

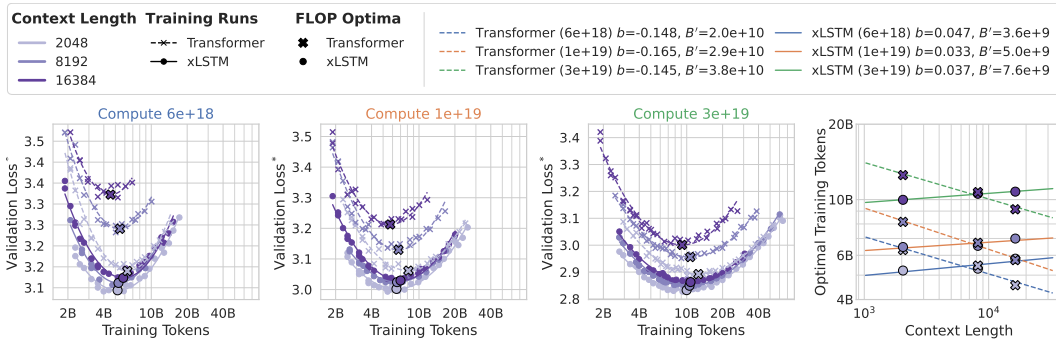


Figure 12: Left: IsoFLOP curves for xLSTM and Llama as a function of training token at 3 different compute budgets. Right: Plot of the power-law fits for the compute optimal number of parameters dependent on the context length  $N^*(T)$ . Colors indicate context length and marker types indicate the model types.

1188  
 1189 **C ACCOUNTING: PARAMETERS, CACHE SIZES, FLOPs, MEMORY**  
 1190 **OPERATIONS**

1191 In this section, we count number of parameters (App. C.1), memory state or KV cache size C.2,  
 1192 FLOPs (App. C.3), and memory operations (App. C.4) for mLSTM models based on the architecture  
 1193 of xLSTM 7B (Beck et al., 2025b) and Transformer models with Self-Attention based on the Llama  
 1194 3 architecture (Grattafiori et al., 2024).

1195 We use the notation defined in Tab. 4.

1196 We start with counting the number of memory operations and FLOPs for matrix multiplication, which  
 1197 is a very common operation in neural networks. A linear layer with input  $\mathbf{X}$  and output  $\mathbf{Y}$  and weight  
 1198 matrix  $\mathbf{W}$  can be written as

$$1200 \quad \mathbf{Y}_{(B \times d_{\text{out}})} = \mathbf{X}_{(B \times d_{\text{in}})} \mathbf{W}^{\top}_{(d_{\text{in}} \times d_{\text{out}})}. \quad (5)$$

1201 This linear layer has  $2Bd_{\text{in}}d_{\text{out}}$  FLOPs:

$$1202 \quad \text{FLOPs}_{\text{linear}} = 2Bd_{\text{in}}d_{\text{out}} \quad (6)$$

1203 In order to compute the output  $\mathbf{Y}$ , we need to read the input  $\mathbf{X}$  and the weights  $\mathbf{W}$  and write the  
 1204 output  $\mathbf{Y}$ . This yields

$$1205 \quad \text{Bytes}_{\text{linear}} = B(d_{\text{in}} + d_{\text{out}}) \times \text{bytes}_{\mathbf{X}} + d_{\text{in}}d_{\text{out}} \times \text{bytes}_{\mathbf{W}} \quad (7)$$

1206 memory operations in loaded and stored bytes. We will use these counts throughout the remainder of  
 1207 this section.

1208 Table 4: **Notation** for FLOP and Memory Operation Counts.

1215 Symbol	1216 Description
1216 $B$	1217 Batch size
1217 $T, (T_p, T_g)$	1218 Sequence length, (prefill length, generation length)
1218 $S$	1219 Query sequence length (only for Self-Attention)
1219 $L$	1220 Chunk size
1220 $d_{\text{hv}}$	1221 Head dimension for values and hidden states
1221 $d_{\text{qk}}$	1222 Head dimension for queries and keys
1222 $d_{\text{model}}$	1223 Model / Embedding dimension
1223 $d_{\text{ff}}$	1224 Feedforward dimension
1224 $p_{\text{ff}}$	1225 Feedforward projection factor
1225 $p_{\text{qk}}$	1226 Query key projection factor
1226 $n_{\text{head},(q)}$	1227 Number of (query) heads
1227 $n_{\text{head},kv}$	1228 Number of key and value heads
1228 $n_{\text{chunk}}$	1229 Number of chunks
1229 $n_{\text{vocab}}$	1230 Vocabulary size
1230 $n_{\text{layer}}$	1231 Number of layers
1231 $F_{\text{OP}}$	1232 FLOPs for the operation OP (e.g. exp)
1232 $F_{\text{causal}}$	1233 Factor that accounts for causality, typically 0.5
1233 $\text{bytes}_{\mathbf{X}}$	1234 Number of bytes used for each element in tensor X

1242 C.1 PARAMETER COUNTS  
12431244 We count the number of parameters of mLSTM models (C.1.1) and Transformer models (C.1.2). We  
1245 include embedding and normalization layer parameters in our parameter counts.  
12461247 C.1.1 mLSTM PARAMS  
12481249 For the mLSTM models, we use the optimized xLSTM architecture from [Beck et al. \(2025b\)](#) and  
1250 count the parameters in Tab. 5.  
12511252 Table 5: **Parameter counts for the mLSTM Model.**  
1253

Parameters	
<b>Embeddings:</b>	$n_{\text{vocab}} d_{\text{model}}$
<i>mLSTM (single layer)</i>	
<b>PreNorm:</b>	$d_{\text{model}}$
<b>QKV:</b>	$d_{\text{model}} n_{\text{head}} (2d_{\text{qk}} + d_{\text{hv}})$
<b>Input &amp; Forget Gates:</b>	$2d_{\text{model}} n_{\text{head}} + 2n_{\text{head}}$
<b>Output Gate:</b>	$d_{\text{model}} n_{\text{head}} d_{\text{hv}}$
<b>Output Norm:</b>	$n_{\text{head}} d_{\text{hv}}$
<b>Output Projection:</b>	$d_{\text{model}} n_{\text{head}} d_{\text{hv}}$
<i>Total mLSTM layer <math>N_{\text{mLSTM,layer}}</math>:</i>	$d_{\text{model}} n_{\text{head}} (2d_{\text{qk}} + d_{\text{hv}} + 2) + 2d_{\text{model}}^2 + 2n_{\text{head}} + 2d_{\text{model}}$
<i>Feedforward (single layer)</i>	
<b>PreNorm:</b>	$d_{\text{model}}$
<b>MLPs:</b>	$3d_{\text{model}} d_{\text{ff}}$
<i>Total Feedforward <math>N_{\text{ff,layer}}</math>:</i>	$3d_{\text{model}} d_{\text{ff}} + d_{\text{model}}$
<b>Output Norm:</b>	$d_{\text{model}}$
<b>Unembedding:</b>	$d_{\text{model}} n_{\text{vocab}}$
<b>Total mLSTM model <math>N_{\text{mLSTM}}</math>:</b>	$n_{\text{layer}} (N_{\text{mLSTM,layer}} + N_{\text{ff,layer}}) + 2d_{\text{model}} n_{\text{vocab}} + d_{\text{model}}$

1274 C.1.2 TRANSFORMER PARAMS  
12751276 For the Transformer models, we assume the Llama architecture with Grouped-Query Attention  
1277 from [Grattafiori et al. \(2024\)](#) and count the parameters in Tab. 6.  
12781279 C.2 MEMORY STATE AND KV-CACHE SIZE  
12801281 In Tab. 7 we list the memory state and KV cache sizes for the mLSTM and Transformer model archi-  
1282 tectures. We compare the mLSTM with standard Multi-Head Attention (MHA) ([Vaswani et al., 2017](#)),  
1283 Grouped-Query Attention (GQA) ([Ainslie et al., 2023](#)) and Multi-Head Latent Attention ([DeepSeek-  
1284 AI, 2024a](#)).1285 In contrast to the KV caches of the attention variants, the mLSTM has a fixed size memory state that  
1286 does not depend on the sequence length  $T$ .  
12871288 We compare the size of the memory state and KV cache sizes in number of elements. To obtain the  
1289 number of bytes, we multiply by number of elements per element bytes $_X$ .  
12901291  
1292  
1293  
1294  
1295

1296 Table 6: **Parameter counts for the Transformer Self-Attention Model.**  
1297

1298 Parameters	1299
<b>1300 Embeddings:</b>	$n_{\text{vocab}} d_{\text{model}}$
<i>1301 Self-Attention (single layer)</i>	
<b>1302 PreNorm:</b>	$d_{\text{model}}$
<b>1303 QKV:</b>	$d_{\text{model}}(d_{\text{qk}} n_{\text{head},\text{q}} + (d_{\text{qk}} + d_{\text{hv}}) n_{\text{head},\text{kv}})$
<b>1304 Output Projection:</b>	$d_{\text{model}} n_{\text{head},\text{q}} d_{\text{hv}}$
<i>1305 Total Attention layer <math>N_{\text{Att},\text{layer}}</math>:</i>	$d_{\text{model}}(d_{\text{qk}} n_{\text{head},\text{q}} + d_{\text{qk}} n_{\text{head},\text{kv}} + d_{\text{hv}} n_{\text{head},\text{kv}}) + d_{\text{model}}^2 + d_{\text{model}}$
<i>1306 Feedforward (single layer)</i>	
<b>1307 PreNorm:</b>	$d_{\text{model}}$
<b>1308 MLPs:</b>	$3d_{\text{model}} d_{\text{ff}}$
<i>1309 Total Feedforward <math>N_{\text{ff},\text{layer}}</math>:</i>	$3d_{\text{model}} d_{\text{ff}} + d_{\text{model}}$
<b>1310 Output Norm:</b>	$d_{\text{model}}$
<b>1311 Unembedding:</b>	$d_{\text{model}} n_{\text{vocab}}$
<b>1312 Total Transformer model <math>N_{\text{Att}}</math>:</b>	$n_{\text{layer}}(N_{\text{Att},\text{layer}} + N_{\text{ff},\text{layer}}) + 2d_{\text{model}} n_{\text{vocab}} + d_{\text{model}}$

1315 Table 7: **Memory State and KV-Cache Sizes for different Sequence-Mix operations.** All terms  
1316 denote the number of elements.  
1317

1318 Sequence Mix Operation	1319 Memory Size in #Elements
1320 Multi-Head Attention (MHA):	$2n_{\text{head},\text{q}} d_{\text{hv}} T$
1321 Grouped-Query Attention (GQA):	$2n_{\text{head},\text{kv}} d_{\text{hv}} T$
1322 Multi-Head Latend Attention (MLA):	$\frac{9}{2} d_{\text{hv}} T$
1323 mLSTM:	$n_{\text{head},\text{q}}(d_{\text{hv}} d_{\text{qk}} + d_{\text{qk}} + 1)$

1325 

### C.3 FLOP COUNTS

1328 In this section, we count the FLOPs for the mLSTM and the Transformer model architecture. For  
1329 each model architecture we count the sequence length dependent FLOPs for the sequence mix layer  
1330 first, i.e. the mLSTM cell (C.3.1) and the Self-Attention layer (C.3.3), and then combine them with  
1331 the FLOPs of the other layers in the model architecture to obtain the total FLOPs for the mLSTM  
1332 (C.3.2) and the Transformer model (C.3.4).

1333 We do not drop subleading terms and set also count FLOPs for all operations equally, i.e.  $F_{\text{OP}} = 1$ .  
1334 We also count the FLOPs for the normalization layers with  $F_{\text{norm}} = 3$  (we assume the factor of 3  
1335 because we have mean, variance and division operations). The skip connection FLOPs are counted  
1336 with  $F_{\text{skip}} = 1$ , or if neglected with  $F_{\text{skip}} = 0$ . Following our training configuration, we use the  
1337 chunkwise-parallel formulation with chunk size  $L = 64$  and  $F_{\text{causal}} = 0.5$  for the FLOP counts and  
1338 scaling laws in the main text.

1339 

#### C.3.1 mLSTM CELL FLOPS

1342 The mLSTM is a linear RNN with gating and can be computed either with a recurrent, a fully parallel  
1343 or a chunkwise-parallel formulation (Beck et al., 2025a). Each of these formulations has a different  
1344 FLOP and memory operation count. For training and for prefill in inference the mLSTM relies  
1345 on the chunkwise-parallel formulation, which parallelizes the computation over the input sequence  
1346 and can therefore fully utilize modern hardware. For generation, the mLSTM uses the recurrent  
1347 formulation, which uses constant compute and memory per generation step (i.e. compute and memory  
1348 requirements are independent of the sequence length).

1349 In this section, we count the number of FLOPs for both the chunkwise-parallel and the recurrent  
formulation of the mLSTM cell.

1350 **Chunkwise-Parallel Formulation (Tab. 8, Eq. 8).** We list the FLOP counts for the individual terms  
 1351 of the chunkwise-parallel mLSTM formulation for a single head and a single chunk in Tab. 8.  
 1352

1353 To obtain the total FLOPs for a full sequence of length  $T$ , we multiply these counts by the number of  
 1354 (query) heads  $n_{\text{head}}$  and chunks  $n_{\text{chunk}} = T/L$ . This yields  
 1355

$$\begin{aligned} \text{FLOPs}_{\text{mLSTM,cwp}} = n_{\text{head}} \times & \left( TLF_{\text{causal}} (2(d_{\text{qk}} + d_{\text{hv}}) + 8) + TL \right. \\ & + 2TF_{\text{causal}} + T (4d_{\text{qk}}d_{\text{hv}} + 6d_{\text{qk}} + 4d_{\text{hv}} + 13) \\ & \left. + \frac{T}{L} (2d_{\text{qk}}d_{\text{hv}} + 2d_{\text{qk}} + 5) \right). \end{aligned} \quad (8)$$

1361 Table 8: **FLOP counts** for the **chunkwise-parallel mLSTM formulation** for mLSTM. All terms  
 1362 denote the FLOP count per head and chunk.  
 1363

FLOPs	Exact	Simplified ( $F_{\text{OP}} = 1$ )
<i>Recurrent computation of the inter chunk states</i>		
<b>Gates:</b>	$2L + \frac{1}{2}L(L + 1) + L(1 + F_{\text{exp}} + F_{\text{log}} + F_{\text{sig}}) + 3 + F_{\text{max}} + F_{\text{exp}}$	$0.5L^2 + 6.5L + 5$
<b>Numerator:</b>	$2d_{\text{qk}}d_{\text{hv}} + 2Ld_{\text{qk}}d_{\text{hv}} + Ld_{\text{qk}}$	$2d_{\text{qk}}d_{\text{hv}} + 2Ld_{\text{qk}}d_{\text{hv}} + Ld_{\text{qk}}$
<b>Denominator:</b>	$2d_{\text{qk}} + 2Ld_{\text{qk}}$	$2d_{\text{qk}} + 2Ld_{\text{qk}}$
<i>Parallel computation of the intra chunk outputs</i>		
<b>Cumulative Forget Gates:</b>	$\frac{1}{2}L(L + 1) + L(F_{\text{log}} + F_{\text{sig}})$	$0.5L^2 + 2.5L$
<b>Gate Matrix:</b>	$F_{\text{causal}} \times \left( \frac{1}{2}L^2(3 + F_{\text{exp}} + F_{\text{max}}) + L(1 + F_{\text{max}}) \right)$	$F_{\text{causal}} \times (5L^2 + 2L)$
<b>Intra Outputs:</b>	$F_{\text{causal}} \times (2L^2(d_{\text{qk}} + d_{\text{hv}}) + 3L^2)$	$F_{\text{causal}} \times (2L^2(d_{\text{qk}} + d_{\text{hv}}) + 3L^2)$
<i>Parallel computation of the inter chunk outputs</i>		
<b>Inter Outputs:</b>	$2Ld_{\text{qk}}d_{\text{hv}} + 3Ld_{\text{qk}}$	$2Ld_{\text{qk}}d_{\text{hv}} + 3Ld_{\text{qk}}$
<i>Combination of inter and intra chunk outputs</i>		
<b>Output Combination:</b>	$2Ld_{\text{hv}} + L(1 + F_{\text{max}} + F_{\text{abs}} + F_{\text{exp}})$	$2Ld_{\text{hv}} + 4L$
<b>Total:</b>	—	$L^2F_{\text{causal}} (2(d_{\text{qk}} + d_{\text{hv}}) + 8) + L^2 + 2LF_{\text{causal}} + L(4d_{\text{qk}}d_{\text{hv}} + 6d_{\text{qk}} + 4d_{\text{hv}} + 13) + (2d_{\text{qk}}d_{\text{hv}} + 2d_{\text{qk}} + 5)$

1380 **Recurrent Formulation (Tab. 9, Eq. 9).** We list the FLOP counts for the individual terms of the  
 1381 recurrent mLSTM formulation for a single head and a single time step in Tab. 9.  
 1382

1383 To obtain the total counts for one generation step, we multiply by the number of heads  $n_{\text{head}}$ . This  
 1384 yields  
 1385

$$\text{FLOPs}_{\text{mLSTM,rec}} = n_{\text{head}} \times (6d_{\text{qk}}d_{\text{hv}} + 7d_{\text{qk}} + d_{\text{hv}} + 12). \quad (9)$$

1386 Table 9: **FLOP counts** for the **recurrent mLSTM formulation** for mLSTM. All terms denote the  
 1387 FLOP count for a single timestep per head.  
 1388

FLOPs	Exact	Simplified ( $F_{\text{OP}} = 1$ )
<b>Gates:</b>	$4 + 2F_{\text{exp}} + F_{\text{log}} + F_{\text{sig}} + F_{\text{max}}$	9
<b>Memory Cell Update:</b>	$4d_{\text{qk}}d_{\text{hv}}$	$4d_{\text{qk}}d_{\text{hv}}$
<b>Denominator &amp; Scale:</b>	$6d_{\text{qk}} + d_{\text{hv}} + 1 + F_{\text{abs}} + F_{\text{max}}$	$6d_{\text{qk}} + d_{\text{hv}} + 3$
<b>Output:</b>	$2d_{\text{hv}}d_{\text{qk}} + d_{\text{qk}}$	$2d_{\text{hv}}d_{\text{qk}} + d_{\text{qk}}$
<b>Total:</b>	—	$6d_{\text{qk}}d_{\text{hv}} + 7d_{\text{qk}} + d_{\text{hv}} + 12$

### 1396 C.3.2 mLSTM MODEL FLOPS

1397 The number of FLOPs for the backbone is identical for training, prefill and generation as the operations  
 1398 (embeddings, linear layers and layernorms) do not depend on the sequence length. Therefore, we  
 1399 count the FLOPs per token for the mLSTM backbone. To obtain the total FLOPs for the specific  
 1400 setting we have to use the respective expression for the mLSTM cell FLOPs from Appendix C.3.1.  
 1401

1402 **mLSTM Backbone (Tab. 10).** We count the FLOPs for the mLSTM backbone for a single token  
 1403 in Tab. 10 and leave the mLSTM cell FLOPs unspecified. The number of tokens for one batch of  
 1404 sequences is  $BT$ .

1404 Table 10: **FLOP counts** for the **mLSTM backbone**. All terms denote the FLOP count per token, i.e.  
 1405 to obtain the FLOPs for one batch we multiply by  $BT$  tokens.

FLOPs	—
<b>Embeddings:</b>	—
<i>mLSTM (single layer)</i>	
<b>PreNorm &amp; Skip:</b>	$d_{\text{model}}(F_{\text{skip}} + F_{\text{norm}})$
<b>QKV:</b>	$2d_{\text{model}}n_{\text{head}}(2d_{\text{qk}} + d_{\text{hv}})$
<b>Input &amp; Forget Gates:</b>	$2d_{\text{model}}n_{\text{head}} + 2n_{\text{head}}$
<b>mLSTM Cell:</b>	$\text{FLOPs}_{\text{mLSTM}}$
<b>Output Gate:</b>	$2d_{\text{model}}n_{\text{head}}d_{\text{hv}} + n_{\text{head}}d_{\text{hv}}F_{\text{sig}}$
<b>Output Norm:</b>	$n_{\text{head}}d_{\text{hv}}F_{\text{norm}}$
<b>Output Projection:</b>	$2d_{\text{model}}n_{\text{head}}d_{\text{hv}}$
<i>Total mLSTM layer FLOPs</i> <sub>mLSTM,layer</sub> :	—
<i>Feedforward (single layer)</i>	
<b>PreNorm &amp; Skip:</b>	$d_{\text{model}}(F_{\text{skip}} + F_{\text{norm}})$
<b>MLPs:</b>	$6d_{\text{model}}d_{\text{ff}}$
<b>Activations:</b>	$d_{\text{ff}}(1 + F_{\text{swish}})$
<i>Total Feedforward FLOPs</i> <sub>ff,layer</sub> :	—
<b>Output Norm:</b>	$d_{\text{model}}F_{\text{norm}}$
<b>Unembedding:</b>	$2d_{\text{model}}n_{\text{vocab}}$
<b>Total mLSTM model FLOPs</b> <sub>mLSTM,model</sub> :	—

### C.3.3 SELF-ATTENTION FLOPS

We count the FLOPs for a single Self-Attention head during training or prefill and generation in Tab. 11. We denote the number of keys and values in the sequence as  $T$ , and the number of queries as  $S$ . During prefill we have  $S = T$ , since the input sequence is processed in parallel and during autoregressive generation we have  $S = 1$ , since we generate one token at a time. We typically use  $F_{\text{softmax}} = 5$  and  $F_{\text{causal}} = 0.5$  following [Busbridge et al. \(2025\)](#) as FLOP factor for softmax (sm).

1437 Table 11: **FLOP counts for Self-Attention**. All terms denote the FLOP count per (query) head.

FLOPs	Generic	Prefill ( $S = T$ )	Generate ( $S = 1$ )
<i>Attention computation</i>			
<b>Logits:</b>	$2STd_{\text{qk}} \times F_{\text{causal}}$	$2T^2d_{\text{qk}} \times F_{\text{causal}}$	$2Td_{\text{qk}} \times F_{\text{causal}}$
<b>Attention:</b>	$STF_{\text{softmax}} \times F_{\text{causal}}$	$T^2F_{\text{softmax}} \times F_{\text{causal}}$	$TF_{\text{softmax}} \times F_{\text{causal}}$
<b>Hiddens/Outputs:</b>	$2STd_{\text{hv}} \times F_{\text{causal}}$	$2T^2d_{\text{hv}} \times F_{\text{causal}}$	$2Td_{\text{hv}} \times F_{\text{causal}}$
<b>Total:</b>	$2STF_{\text{causal}}(d_{\text{qk}} + d_{\text{hv}} + 0.5F_{\text{sm}})$	$2T^2F_{\text{causal}}(d_{\text{qk}} + d_{\text{hv}} + 0.5F_{\text{sm}})$	$2TF_{\text{causal}}(d_{\text{qk}} + d_{\text{hv}} + 0.5F_{\text{sm}})$

1446 **Self-Attention in Training (forward only) and Prefill (Eq. 10).** To obtain the FLOPs for all  
 1447 Self-Attention heads for a full sequence  $T$  or  $T_p$ , we multiply by the number of (query) heads  $n_{\text{head},q}$   
 1448 and the number of tokens  $T$ . This yields

$$1449 \text{FLOPs}_{\text{Att,train-pref}} = 2F_{\text{causal}}T^2n_{\text{head},q}(d_{\text{qk}} + d_{\text{hv}} + 0.5F_{\text{sm}}). \quad (10)$$

1451 **Self-Attention FLOPs in Generation (Eq. 16).** During generation the number of FLOPs per token  
 1452 is dependent on the number of previous tokens  $T = T_p + t_g$ , where  $T_p$  is the number of prefill tokens  
 1453 and  $t_g$  is the number of generated tokens so far. We denote the number of total tokens to be generated  
 1454 as  $T_g$ . To obtain the FLOP counts for the  $t_g$ -th generated token, we need to multiply the FLOPs for  
 1455 the Self-Attention layer by the number of (query) heads  $n_{\text{head},q}$ . We obtain the FLOPs for the  $t_g$ -th  
 1456 generated token as

$$1457 \text{FLOPs}_{\text{Att,gen-step}}(t_g) = 2F_{\text{causal}}n_{\text{head},q}(d_{\text{qk}} + d_{\text{hv}} + 0.5F_{\text{sm}})(T_p + t_g). \quad (11)$$

With  $a = 2F_{\text{causal}}n_{\text{head},q}(d_{\text{qk}} + d_{\text{hv}} + 0.5F_{\text{sm}})$  we can compute the total FLOPs for  $T_g$  generated tokens as the sum of FLOPs for each generated token as

$$\text{FLOPs}_{\text{Att,gen-seq}} = \sum_{t_g=1}^{T_g} \text{FLOPs}_{\text{Att,gen-step}}(t_g) \quad (12)$$

$$= \sum_{t_g=1}^{T_g} (aT_p + at_g) \quad (13)$$

$$= aT_p T_g + a \sum_{t_g=1}^{T_g} t_g \quad (14)$$

$$= aT_p T_g + \frac{1}{2} aT_g(T_g + 1). \quad (15)$$

As a result we obtain the total FLOPs with a prefill or prompt length  $T_p$  and a total number of generated tokens  $T_g$  as

$$\text{FLOPs}_{\text{Att,gen-seq}} = 2F_{\text{causal}}n_{\text{head},q}(d_{\text{qk}} + d_{\text{hv}} + 0.5F_{\text{sm}}) \left( T_p T_g + \frac{1}{2} T_g(T_g + 1) \right). \quad (16)$$

### C.3.4 TRANSFORMER MODEL FLOPS

Similar to the mLSTM backbone in Appendix C.3.2, the number of FLOPs for the Transformer backbone is identical for training, prefill and generation as the operations (embeddings, linear layers and layernorms) do not depend on the sequence length. Therefore, we count the FLOPs per token for the Transformer backbone. To obtain the total FLOPs for the specific setting we have to use the respective expression for the Self-Attention layer FLOPs from Appendix C.3.3.

**Transformer Backbone (Tab. 12).** We count the FLOPs for the Transformer backbone for a single token in Tab. 12 and leave the Self-Attention FLOPs unspecified. The number of tokens for one batch of sequences is  $BT$ .

Table 12: **FLOP counts for the Transformer backbone.** All terms denote the FLOP count per token, i.e. to obtain the FLOPs for one batch we multiply by  $BT$  tokens.

FLOPs	
<b>Embeddings:</b>	—
<i>Attention (single layer)</i>	
<b>PreNorm &amp; Skip:</b>	$d_{\text{model}}(F_{\text{skip}} + F_{\text{norm}})$
<b>QKV:</b>	$2d_{\text{model}}(d_{\text{qk}}n_{\text{head},q} + d_{\text{qk}}n_{\text{head},kv} + d_{\text{hv}}n_{\text{head},kv})$
<b>Attention:</b>	$\text{FLOPs}_{\text{Att}}$
<b>Output Projection:</b>	$2d_{\text{model}}n_{\text{head},q}d_{\text{hv}}$
<i>Total Attention layer FLOPs<sub>Att,layer</sub>:</i>	—
<i>Feedforward (single layer)</i>	
<b>PreNorm &amp; Skip:</b>	$d_{\text{model}}(F_{\text{skip}} + F_{\text{norm}})$
<b>MLPs:</b>	$6d_{\text{model}}d_{\text{ff}}$
<b>Activations:</b>	$d_{\text{ff}}(1 + F_{\text{swish}})$
<i>Total Feedforward FLOPs<sub>ff,layer</sub>:</i>	—
<b>Output Norm:</b>	$d_{\text{model}}F_{\text{norm}}$
<b>Unembedding:</b>	$2d_{\text{model}}n_{\text{vocab}}$
<b>Total Transformer model FLOPs<sub>Att,model</sub>:</b>	—

1512 C.4 MEMORY OPERATION COUNTS  
1513

1514 In this section, we count the memory operations for the mLSTM and the Transformer model architecture.  
1515 We follow the same outline as for the FLOP counts in Appendix C.3 and first count the memory  
1516 operations for the mLSTM cell (C.4.1) and the Self-Attention layer (C.4.3), and then combine them  
1517 with the memory operations of the other layers in the model backbone to obtain the total memory  
1518 operations for the mLSTM (C.4.2) and the Transformer model (C.4.4). We model weight MemOps  
1519 as a one-time streaming cost (perfect on-chip reuse), i.e., independent of the number of token in the  
1520 batch  $BT$ . This is reasonable with persistent/fused kernels and per-rank weight matrices that fit in  
1521 on-chip cache. Depending on the exact experimental configuration, this assumption might not hold as  
1522 we observe when modeling the step time through MemOps in Section D.3.

1523 We include the memory operation count for the normalization layers, but can neglect them by setting  
1524  $\text{bytes}_{\text{norm}} = 0$  and  $\text{bytes}_{\text{act},\text{norm}} = 0$ .

1525 C.4.1 mLSTM CELL MEMOPS  
1526

1527 Similar to the FLOP counts in Appendix C.3.1, we count the memory operations for the mLSTM cell  
1528 for both the chunkwise-parallel and the recurrent formulation.

1529 **Chunkwise-Parallel Formulation (Tab. 13, Eq. 17).** The implementation of the chunkwise-parallel  
1530 mLSTM formulation consists of two kernels (Beck et al., 2025a). We count the memory operations  
1531 for the loading and storing of the inputs and outputs of each kernel for a single chunk and head in  
1532 Tab. 13.

1533 By multiplying with the number of heads  $n_{\text{head}}$  and the number of chunks  $n_{\text{chunk}} = T/L$ , we obtain  
1534 the total memory operation counts for the chunkwise-parallel mLSTM formulation as  
1535

$$1536 \text{Bytes}_{\text{mLSTM,cwp}} = n_{\text{head}} \frac{T}{L} (4L \times \text{bytes}_{\text{if}} + 3L(d_{\text{hv}} + d_{\text{qk}}) \times \text{bytes}_{\text{qkv}} \\ 1537 + 2n_{\text{head}}(L + d_{\text{hv}}d_{\text{qk}} + d_{\text{qk}} + 1) \times \text{bytes}_{C_{mn}}). \quad (17)$$

1540  
1541 Table 13: **Memory operation counts for the chunkwise-parallel mLSTM formulation.** All terms  
1542 denote the memory operation count per head and chunk.

Bytes	
<i>Inter-chunk Recurrent Kernel</i>	
<b>Load:</b>	$L(d_{\text{qk}} + d_{\text{hv}}) \times \text{bytes}_{\text{qkv}} + 2L \times \text{bytes}_{\text{if}}$
<b>Store:</b>	$(d_{\text{qk}}d_{\text{hv}} + d_{\text{qk}} + 1) \times \text{bytes}_{C_{nm}}$
<i>Intra-chunk Parallel Kernel</i>	
<b>Load:</b>	$L(2d_{\text{qk}} + d_{\text{hv}}) \times \text{bytes}_{\text{qkv}} + 2L \times \text{bytes}_{\text{if}} \\ + (d_{\text{qk}}d_{\text{hv}} + d_{\text{qk}} + 1) \times \text{bytes}_{C_{nm}}$
<b>Store:</b>	$Ld_{\text{hv}} \times \text{bytes}_{\text{qkv}} + 2L \times \text{bytes}_{C_{nm}}$
<b>Total:</b>	$4L \times \text{bytes}_{\text{if}} \\ + 3L(d_{\text{hv}} + d_{\text{qk}}) \times \text{bytes}_{\text{qkv}} \\ + 2(L + d_{\text{hv}}d_{\text{qk}} + d_{\text{qk}} + 1) \times \text{bytes}_{C_{mn}}$

1555 **Recurrent Formulation (Tab. 14, Eq. 18).** During text generation we use the recurrent formulation,  
1556 which loads the previous memory state and the current input and stores the output and the next  
1557 memory state. We obtain the total memory operation counts for the recurrent mLSTM formulation  
1558 by multiplying the counts in Tab. 14 with the number of heads  $n_{\text{head}}$ .

1559  $\text{Bytes}_{\text{mLSTM,rec}} = n_{\text{head}} \times (2 \times \text{bytes}_{\text{if}} + 2(d_{\text{hv}} + d_{\text{qk}}) \times \text{bytes}_{\text{qkv}} + 2d_{\text{hv}}d_{\text{qk}} \times \text{bytes}_{C_{mn}}). \quad (18)$   
1560

1562 C.4.2 mLSTM MODEL MEMOPS  
1563

1564 The memory operations of each layer of the backbone (excluding the mLSTM cell) consist of the input  
1565 and output activations as well as the parameters. The inputs and outputs depend on the number of  
tokens  $BT$  in the batch, whereas the parameters are independent of the number of tokens.

1566 Table 14: **Memory operation counts** for the **recurrent mLSTM formulation**. All terms denote  
 1567 the memory operation count for a single timestep per head. We assume the states are materialized at  
 1568 every timestep.

Bytes	
<b>Load:</b>	$(2d_{\text{qk}} + d_{\text{hv}}) \times \text{bytes}_{\text{qkv}} + 2 \times \text{bytes}_{\text{if}}$ $+ (d_{\text{qk}}d_{\text{hv}} + d_{\text{qk}} + 1) \times \text{bytes}_{Cmn}$
<b>Store:</b>	$d_{\text{hv}} \times \text{bytes}_{\text{qkv}} + (d_{\text{qk}}d_{\text{hv}} + d_{\text{qk}} + 1) \times \text{bytes}_{Cmn}$
<b>Total:</b>	$2 \times \text{bytes}_{\text{if}} + 2(d_{\text{hv}} + d_{\text{qk}}) \times \text{bytes}_{\text{qkv}}$ $+ 2d_{\text{hv}}d_{\text{qk}} \times \text{bytes}_{Cmn}$

1579 The total memory operations for each layer are the sum of the memory operations for the input and  
 1580 output activations and the parameters and are given in Tab. 15. By default, we assume that all weights  
 1581 are stored in the same precision and use the same number of bytes  $\text{bytes}_W$  for all weights.

1582 Table 15: **Memory Operation counts** for the **mLSTM Model**.

Memory Ops in bytes	Input & Output Activations	Weights
<b>Embeddings:</b>	$BTn_{\text{vocab}}d_{\text{model}} \times \text{bytes}_{W_{\text{emb}}}$	
<i>mLSTM (single layer)</i>		
<b>PreNorm:</b>	$BTd_{\text{model}} \times \text{bytes}_{\text{act},\text{norm}}$	$d_{\text{model}} \times \text{bytes}_{W_{\text{norm}}}$
<b>QKV:</b>	$BT(d_{\text{model}} + n_{\text{head}}(2d_{\text{qk}} + d_{\text{hv}})) \times \text{bytes}_{\text{qkv}}$	$d_{\text{model}}n_{\text{head}}(2d_{\text{qk}} + d_{\text{hv}}) \times \text{bytes}_{W_{\text{qkv}}}$
<b>Input &amp; Forget Gates:</b>	$2BT(d_{\text{model}} + n_{\text{head}}) \times \text{bytes}_{\text{if}}$	$(2d_{\text{model}}n_{\text{head}} + 2n_{\text{head}}) \times \text{bytes}_{W_{\text{if}}}$
<b>mLSTM Cell:</b>	$\text{Bytes}_{\text{mLSTM}}$	—
<b>Output Gate:</b>	$BT(d_{\text{model}} + n_{\text{head}}d_{\text{hv}}) \times \text{bytes}_{\text{act}}$	$d_{\text{model}}n_{\text{head}}d_{\text{hv}} \times \text{bytes}_{W_o}$
<b>Output Norm:</b>	$BTn_{\text{head}}d_{\text{hv}} \times \text{bytes}_{\text{act},\text{norm}}$	$n_{\text{head}}d_{\text{hv}} \times \text{bytes}_{W_{\text{norm}}}$
<b>Output Projection:</b>	$BT(d_{\text{model}} + n_{\text{head}}d_{\text{hv}}) \times \text{bytes}_{\text{act}}$	$d_{\text{model}}n_{\text{head}}d_{\text{hv}} \times \text{bytes}_{W_{\text{out}}}$
<i>Total mLSTM layer Bytes<sub>mLSTM,layer</sub>:</i>	—	
<i>Feedforward (single layer)</i>		
<b>PreNorm:</b>	$BTd_{\text{model}} \times \text{bytes}_{\text{act},\text{norm}}$	$d_{\text{model}} \times \text{bytes}_{W_{\text{norm}}}$
<b>MLPs:</b>	$3BT(d_{\text{model}} + d_{\text{ff}}) \times \text{bytes}_{\text{act},\text{ff}}$	$3d_{\text{model}}d_{\text{ff}} \times \text{bytes}_{W_{\text{ff}}}$
<i>Total Feedforward Bytes<sub>ff,layer</sub>:</i>	—	
<b>Output Norm:</b>	$BTd_{\text{model}} \times \text{bytes}_{\text{act},\text{norm}}$	$d_{\text{model}} \times \text{bytes}_{W_{\text{norm}}}$
<b>Unembedding:</b>	$BT(d_{\text{model}} + n_{\text{vocab}}) \times \text{bytes}_{\text{act}}$	$d_{\text{model}}n_{\text{vocab}} \times \text{bytes}_{W_{\text{emb}}}$
<i>Total mLSTM model <math>N_{\text{mLSTM}}</math>:</i>	—	

## 1602 C.4.3 SELF-ATTENTION MEMOPS

1603 Similar to the FLOP counts in Appendix C.3.3, we count the memory operations for a single  
 1604 Self-Attention head during training or prefill and generation.1605 These two cases have very different memory operation counts, as during training and prefill we need  
 1606 to load the full sequence of tokens only once, whereas during autoregressive generation we have to  
 1607 load all previous tokens  $T_p + t_g$  (i.e. the whole KV cache) for each generated token.1608 We consider FlashAttention implementations for the Self-Attention operation (Dao, 2024), where the  
 1609 Attention logits are not materialized in HBM. Therefore, we only count the memory operations for  
 1610 loading the query, key and value inputs and the output of Self-Attention in Tab. 16.1611 **Self-Attention in Training and Prefill (Eq. 19).** During training and prefill we need to load the full  
 1612 sequence of  $T$  or  $T_p$  tokens only once. The total memory operation counts are given by

1613 
$$\text{Bytes}_{\text{Att,train-pref}} = (T(d_{\text{qk}} + d_{\text{hv}})(n_{\text{head},\text{q}} + n_{\text{head},\text{kv}})) \times \text{bytes}_{\text{qkv}}. \quad (19)$$

1614 **Self-Attention in Generation (Eq. 21).** Similar to the FLOP counts in Appendix C.3.3, also the  
 1615 memory operation counts for the Self-Attention layer during generation depend on the number of  
 1616 previous tokens  $T = T_p + t_g$ , where  $T_p$  is the number of prefill tokens and  $t_g$  is the number of  
 1617 generated tokens so far.

1620 Table 16: **Memory operation counts for FlashAttention.** For training and prefill  $T = S$ , while for  
 1621 generation  $S = 1$ .

1622

Bytes	Generic
<b>Load:</b>	$(Sd_{\text{qk}}n_{\text{head},\text{q}} + T(d_{\text{qk}} + d_{\text{hv}})n_{\text{head},\text{kv}}) \times \text{bytes}_{\text{qkv}}$
<b>Store:</b>	$Sd_{\text{hv}}n_{\text{head},\text{q}} \times \text{bytes}_{\text{qkv}}$
<b>Total:</b>	$(S(d_{\text{qk}} + d_{\text{hv}})n_{\text{head},\text{q}} + T(d_{\text{qk}} + d_{\text{hv}})n_{\text{head},\text{kv}}) \times \text{bytes}_{\text{qkv}}$

1623

1630 The number of memory operations for the  $t_g$ -th generated token is given by

1631

$$\text{Bytes}_{\text{Att,gen-step}}(t_g) = ((d_{\text{qk}} + d_{\text{hv}})n_{\text{head},\text{q}} + (T_p + t_g)(d_{\text{qk}} + d_{\text{hv}})n_{\text{head},\text{kv}}) \times \text{bytes}_{\text{qkv}} \quad (20)$$

1633

1634 Similar to equations (12)-(15), we can compute the total number of memory operations for  $T_g$   
 1635 generated tokens by summing up the per-step memory operations

1636

$$\begin{aligned} \text{Bytes}_{\text{Att,gen-seq}} = \text{bytes}_{\text{qkv}} \times & \left( T_g(d_{\text{qk}} + d_{\text{hv}})n_{\text{head},\text{q}} \right. \\ & \left. + (T_p T_g + \frac{1}{2} T_g(T_g + 1))(d_{\text{qk}} + d_{\text{hv}})n_{\text{head},\text{kv}} \right) \end{aligned} \quad (21)$$

1639

#### 1641 C.4.4 TRANSFORMER MODEL MEMOPS

1642

1643 Similar to the mLSTM backbone in Appendix C.4.2, the number of memory operations for the  
 1644 Transformer backbone (excluding the Self-Attention layer) consist of the input and output activations  
 1645 as well as the parameters. The memory operations for input and output activations depend on the  
 1646 number of tokens  $BT$  in the batch, whereas the parameters are independent of the number of tokens.

1647

1648 The total memory operations for each layer are the sum of the memory operations for the input and  
 1649 output activations and the parameters and are given in Tab. 17. By default, we assume that all weights  
 1650 are stored in the same precision and use the same number of bytes  $\text{bytes}_W$  for all weights.

1651

Table 17: **Memory Operation counts for the Transformer Model.**

1652

Memory Ops in bytes	Input & Output Activations	Weights
<b>Embeddings:</b>	$BTn_{\text{vocab}}d_{\text{model}} \times \text{bytes}_{W_{\text{emb}}}$	
<i>Attention (single layer)</i>		
<b>PreNorm:</b>	$BTd_{\text{model}} \times \text{bytes}_{\text{act, norm}}$	$d_{\text{model}} \times \text{bytes}_{W_{\text{norm}}}$
<b>QKV:</b>	$BT(d_{\text{model}} + n_{\text{head}}(2d_{\text{qk}} + d_{\text{hv}})) \times \text{bytes}_{\text{qkv}}$	$d_{\text{model}}(d_{\text{qk}}n_{\text{head},\text{q}} + (d_{\text{qk}} + d_{\text{hv}})n_{\text{head},\text{kv}}) \times \text{bytes}_{W_{\text{qkv}}}$
<b>Attention:</b>	$\text{Bytes}_{\text{Att}}$	
<b>Output Projection:</b>	$BT(d_{\text{model}} + n_{\text{head},\text{q}}d_{\text{hv}}) \times \text{bytes}_{\text{act}}$	$d_{\text{model}}n_{\text{head},\text{q}}d_{\text{hv}} \times \text{bytes}_{W_{\text{out}}}$
<i>Total Attention layer Bytes<sub>Att,layer</sub>:</i>	—	
<i>Feedforward (single layer)</i>		
<b>PreNorm:</b>	$BTd_{\text{model}} \times \text{bytes}_{\text{act, norm}}$	$d_{\text{model}} \times \text{bytes}_{W_{\text{norm}}}$
<b>MLPs:</b>	$3BT(d_{\text{model}} + d_{\text{ff}}) \times \text{bytes}_{\text{act,ff}}$	$3d_{\text{model}}d_{\text{ff}}\text{bytes}_{W_{\text{ff}}}$
<i>Total Feedforward Bytes<sub>ff,layer</sub>:</i>	—	
<b>Output Norm:</b>	$BTd_{\text{model}} \times \text{bytes}_{\text{act, norm}}$	$d_{\text{model}} \times \text{bytes}_{W_{\text{norm}}}$
<b>Unembedding:</b>	$BT(d_{\text{model}} + n_{\text{vocab}}) \times \text{bytes}_{\text{act}}$	$d_{\text{model}}n_{\text{vocab}} \times \text{bytes}_{W_{\text{emb}}}$
<b>Total Transformer model <math>N_{\text{Att}}</math>:</b>	—	

1666

1667

1668

1669

1670

1671

1672

1673

## 1674 D MODELING INFERENCE CHARACTERISTICS 1675

1676 In this section, we create a model of the theoretical runtimes of operations in the xLSTM and  
1677 Transformer model architectures to model their inference characteristics (TTFT and step time). This  
1678 theoretical model is based on the FLOP and the memory operation counts in Appendix C.

1679 This theoretical model of inference characteristics has two purposes: First, it allows to investigate the  
1680 theoretical differences in maximal inference speed between xLSTM and Transformer architectures  
1681 and explain the empirically observed behavior. Second, based on TTFT and step time measurements  
1682 for specific architecture configurations, it allows to predict the theoretical inference speed for other  
1683 (possibly larger) configurations and take this into account for selecting the optimal architecture  
1684 configuration based on our scaling laws. This is important if there are certain requirements on  
1685 maximal TTFTs or step times for a particular use-case. With this theoretical model, it is easily  
1686 possible to determine model configurations which satisfy those conditions.

### 1687 D.1 BACKGROUND: THEORETICAL RUNTIME

1688 In order to estimate the total theoretical runtime of workloads on GPUs or TPUs, we can break down  
1689 the runtime into three components (Austin et al., 2025, Part 1):

- 1692 • **Compute time**  $\tau_{\text{FLOPs}}$ : The time it takes to perform the FLOPs of the workload on the  
1693 GPU(s).
- 1694 • **Memory time**  $\tau_{\text{mem}}$ : The time for memory loads and stores from and to GPU memory  
1695 during a workload.
- 1696 • **Communication time**  $\tau_{\text{comm}}$ : The time for communicating or transferring data (e.g. inter-  
1697 mediate results) between multiple GPUs taking part in a workload.

1698 Given the number of floating point operations  $\text{FLOPs}_{\text{algo}}$ , the number of bytes  $\text{Bytes}_{\text{mem,algo}}$  that must  
1699 be loaded and stored, and the number of bytes  $\text{Bytes}_{\text{comm,algo}}$  that must be communicated between  
1700 GPUs, we can compute the individual runtimes as

$$1702 \tau_{\text{FLOPs,algo}} = \frac{\text{FLOPs}_{\text{algo}}}{\alpha_{\text{acc}}}, \quad \tau_{\text{mem,algo}} = \frac{\text{Bytes}_{\text{mem,algo}}}{\beta_{\text{acc}}} \quad \text{and} \quad \tau_{\text{comm,algo}} = \frac{\text{Bytes}_{\text{comm,algo}}}{\gamma_{\text{Bytes}}}, \quad (22)$$

1703 where  $\alpha_{\text{acc}}$ ,  $\beta_{\text{acc}}$  and  $\gamma_{\text{Bytes}}$  are the accelerator specific compute speed in FLOPs/s, the accelerator  
1704 memory bandwidth in Bytes/s and the accelerator communication bandwidth in Bytes/s, respectively.

1705 For accelerator speed  $\alpha_{\text{acc}}$ , accelerator memory bandwidth  $\beta_{\text{acc}}$ , and accelerator communication  
1706 bandwidth  $\gamma_{\text{Bytes}}$ , we use the hardware specifications of NVIDIA V100<sup>2</sup>, A100<sup>3</sup>, H100<sup>4</sup> and B200<sup>5</sup>  
1707 GPUs, which we summarize in Tab. 18.

1708 **Table 18: Hardware Accelerator Specification** for NVIDIA GPUs used in this analysis. Values  
1709 without sparsity. If only the value with sparsity is known, we divide by 2.

1714 GPU	1715 Year	1716 bfloat16 [FLOPs/s]	1717 Memory Bandwidth [Byte/s]	1718 Arithmetic Intensity [FLOPs/byte]	1719 Communication Bandwidth [Byte/s]
1720 V100 SXM2	2017	120e12	0.9e12	133	0.3e12
1721 A100 SXM	2020	312e12	2.039e12	161	0.6e12
1722 H100 SXM	2022	989e12	3.35e12	295	0.9e12
1723 B200 HGX	2025	2250e12	7.7e12	292	1.8e12

1724 If there is no overlap between computation and memory or communication operations, or in other  
1725 words if we cannot load, store or communicate data while the GPU is doing FLOPs, the total runtime

1726 <sup>2</sup><https://www.nvidia.com/en-au/data-center/v100/>

1727 <sup>3</sup><https://www.nvidia.com/en-us/data-center/a100/>

1728 <sup>4</sup><https://www.nvidia.com/en-au/data-center/h100/>

1729 <sup>5</sup><https://resources.nvidia.com/en-us-blackwell-architecture/datasheet>

1728 is the sum of the two, i.e.

$$\tau_{\text{algo,upper}} = \tau_{\text{FLOPs,algo}} + \tau_{\text{mem/comm,algo}}. \quad (23)$$

1729 If the computation and memory or communication operations can be overlapped (i.e. happen in  
1730 parallel), the total runtime is the maximum of the two, i.e.

$$\tau_{\text{algo,lower}} = \max(\tau_{\text{FLOPs,algo}}, \tau_{\text{mem/comm,algo}}). \quad (24)$$

1731 This means the runtime is lower bounded by the maximum of the two and upper bounded by their  
1732 sum (Austin et al., 2025, Part 1).

1733 **Roofline model.** A helpful model for determining whether runtime is bounded by computation  
1734 (compute-bound) or by memory/bandwidth (memory-bound) is the roofline model (Williams et al.,  
1735 2009), see Figure 13 for an illustration. The roofline relates the attainable FLOPs/s with the arithmetic  
1736 intensity  $I_{\text{algo}}$  of the operation performed on the GPU which is given by

$$I_{\text{algo}} = \frac{\text{FLOPs}_{\text{algo}}}{\text{Bytes}_{\text{algo}}}. \quad (25)$$

1737 Thus, the arithmetic intensity is the FLOPs per byte for a given operation. When the arithmetic  
1738 intensity of operations increases, the attainable FLOPs/s increase linearly - operations are essentially  
1739 memory-bound; the GPU has to wait for bytes to arrive to perform calculations. In this setting, the  
1740 runtime is effectively given by  $\tau_{\text{mem/comm,algo}}$ .

1741 Upon reaching the arithmetic intensity of the accelerator  $I_{\text{acc}}$  (see  
1742 Tab. 18 for specifications for common GPU types), the “roofline”  
1743 is reached and operations are essentially compute bound; the  
1744 GPU still performs calculations while the next inputs are ready.  
1745 In this setting, the runtime is effectively given by  $\tau_{\text{FLOPs,algo}}$ .

1746 **Inference stages.** As outlined in Section 4, inference with LLMs  
1747 is typically split into two stages, prefill and generation.

1748 For the *prefill stage*, the TTFT is the key performance metric  
1749 which is the runtime of the LLM in processing an input sequence  
1750 if a certain prefill length, building up caches (Transformer) /  
1751 memory cells (xLSTM) and generating the first token. Following  
1752 Austin et al. (2025, Part 7), we assume that even at relatively low prefill lengths of 256, inference is  
1753 dominated by large matrix multiplications for both Transformers and xLSTM and therefore consider  
1754 the prefill stage to be compute bound. While this might not perfectly model very small prefill lengths,  
1755 those are generally dominated by constant overheads.

1756 For the *generation stage*, step time is the key performance metric which is the runtime of the LLM  
1757 in generating a new token after having processed the the whole input sequence up to the last token.  
1758 This means that during a forward pass, only a tiny amount of compute is necessary to account for this  
1759 new token. However, for Transformers it is necessary to load from the KV cache, which is a very  
1760 bandwidth-intensive operations, followed by streaming weights and storing and loading activations  
1761 for both architectures. Consequently, arithmetic intensities during generation are generally rather  
1762 low (see also Austin et al., 2025, Part 7). We thus assume that during the generation stage, both  
1763 Transformers and xLSTM are memory bound.

## 1771 D.2 PREFILL STAGE: TIME TO FIRST TOKEN

1772 As we assume to be compute bound during prefill, we model the runtime of the prefill stage which  
1773 corresponds to the TTFT as (c.f. Eq. (4)):

$$\tau_{\text{FLOPs,algo}} = \frac{\text{FLOPs}_{\text{algo}}}{\alpha_{\text{eff}}} + \epsilon. \quad (26)$$

1774 FLOPs<sub>algo</sub> can be calculated analytically given the FLOPs calculations provided in Appendix C.3,  
1775  $\alpha_{\text{eff}}$  and  $\epsilon$  need to be fitted using the measured data. Exemplarily, we show the runtimes fitted for the  
1776 measured TTFT in Figure 14 (Transfomer) and Figure 15 (xLSTM) for different model sizes. We fit  
1777  $\alpha_{\text{eff}}$  and  $\epsilon$  per model configuration on TTFTs obtained under various combinations of batch sizes  
1778 and prefill lengths. Our fits show excellent agreement between the predictions from our quantitative

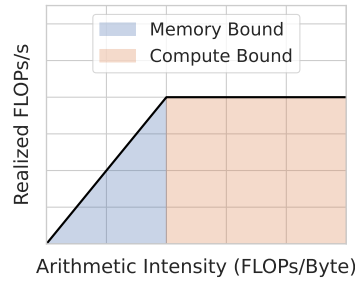


Figure 13: Roofline model.

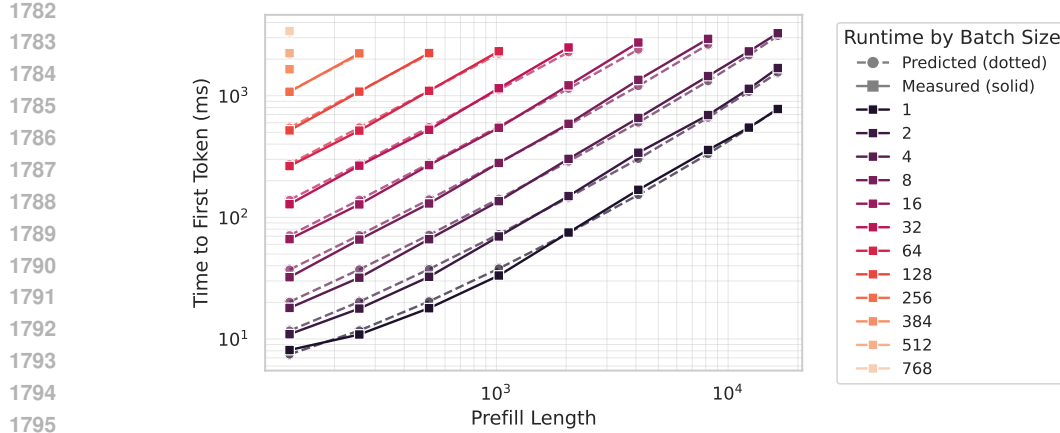


Figure 14: Time to first token, measured and fitted, for a 7B Transformer model as a function of prefill for different batch sizes.

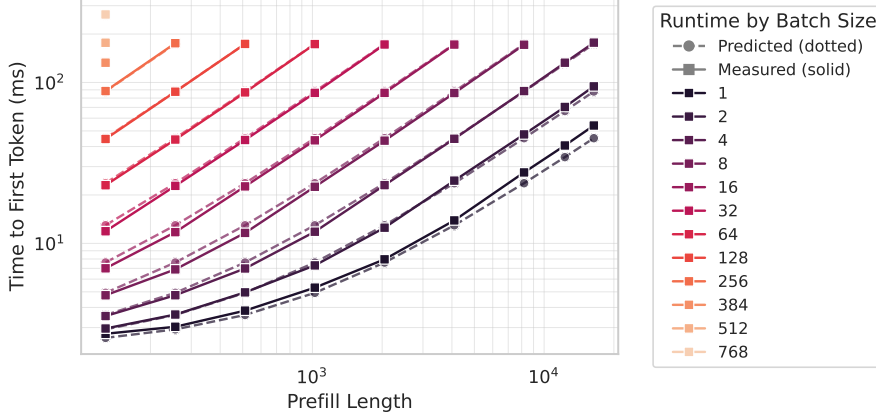


Figure 15: Time to first token, measured and fitted, for a 400M xLSTM model as a function of prefill for different batch sizes.

runtime model and the measured data. In Figure 16 we further show the quotient of the fitted  $\alpha_{\text{eff}}$  and the hardware parameter  $\alpha_{\text{acc}}$  for all model sizes. If  $\alpha_{\text{eff}}/\alpha_{\text{acc}} = 1$ , the hardware would be perfectly utilized according to our model. We see that for both Transformers and xLSTM, the quotient increases, thus larger models utilize the hardware better. Furthermore, both models show relatively similar trends and magnitudes, indicating that the empirical measurement setup allowed for a fair comparison.

### D.3 GENERATION STAGE: STEP TIME

As we assume to be memory-bound during generation stage, we model the runtime of the generation stage which corresponds to the step time as (c.f. Eq. 4):

$$\tau_{\text{mem,algo}} = \frac{\text{Bytes}_{\text{mem,algo}}}{\beta_{\text{eff}}} + \epsilon. \quad (27)$$

$\text{Bytes}_{\text{mem,algo}}$  can be calculated analytically given the MemOps calculations provided in Appendix C.4,  $\beta_{\text{eff}}$  and  $\epsilon$  need to be fitted using the measured data. Furthermore, we found that the fit quality for Transformer further improved by fitting another constant that scales with the batch size. Exemplarily, we show the runtimes fitted for the measured step times in Figure 17 (Transformer) and Figure 18 (xLSTM) for different model sizes. Again, we find a very good agreement between the predictions from our quantitative runtime model and the measured data.

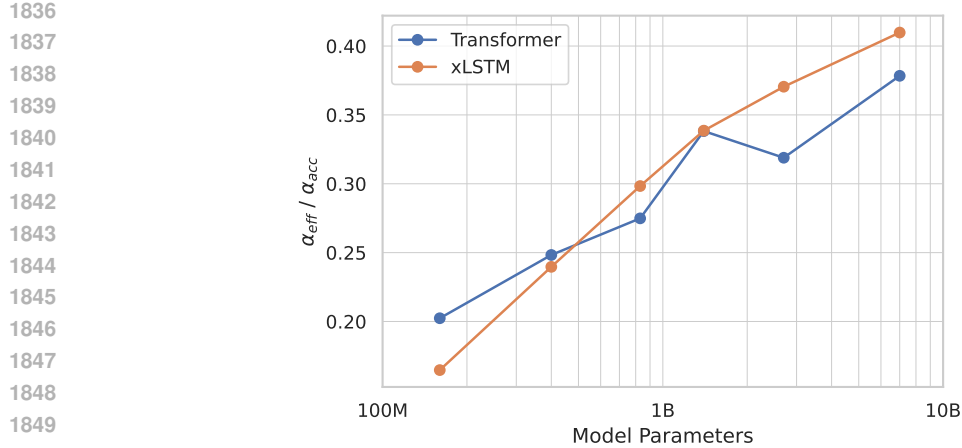


Figure 16: Comparing the fitted  $\alpha_{\text{eff}}$  to the accelerator  $\alpha_{\text{acc}}$  ( $989e12$  for a H100 see Tab. 18). With our experimental setup, we attain similar effective FLOPs for both the Transformer and xLSTM. As expected, the accelerator is better utilized by larger models.

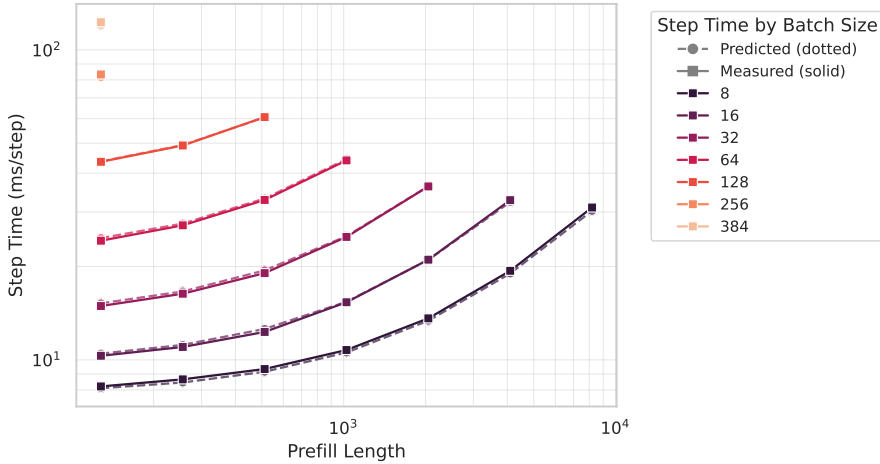


Figure 17: Step time, measured and fitted, for a 7B Transformer model as a function of prefill for different batch sizes.

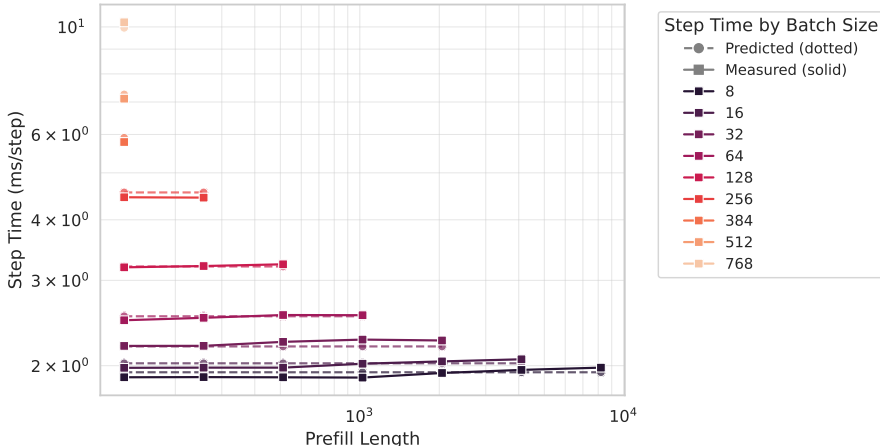


Figure 18: Step time, measured and fitted, for a 400M xLSTM model as a function of prefill for different batch sizes.

1890 **E MODEL CONFIGURATIONS**  
 1891

1892 In this section, we list the model hyperparameters and sizes of all training runs in Token/Param  
 1893 (Sec. E.1) and IsoFLOP (Sec. E.2) of the dataset for our scaling law study.  
 1894

1895 **E.1 MODEL SIZES AND HYPERPARAMETERS IN TOKEN/PARAM CONFIGURATION**  
 1896

1897 **Table 19: List of hyperparameters for xLSTM models** trained with the **Token/Param** configuration  
 1898 with context length  $T = 8192$ .  
 1899

#Params (M)	$d_{\text{model}}$	$d_{\text{ff}}$	$d_{\text{qk}}$	$d_{\text{hv}}$	$n_{\text{heads}}$	$n_{\text{layer}}$	$B$ (seqs)	LR
164	768	2112	64	128	6	12	128	3e-3
406	1024	2752	128	256	4	24	128	3e-3, 1e-3
841	1536	4160	192	384	4	24	256	1e-3, 8e-4
1420	2048	5504	256	512	4	24	256	8e-4, 7e-4
2780	2560	6848	256	512	5	32	512	7e-4
6865	4096	10944	256	512	8	32	256, 512	5e-4, 4e-4

1900  
 1901  
 1902  
 1903  
 1904  
 1905  
 1906  
 1907  
 1908  
 1909 **Table 20: List of hyperparameters for Transformer models** trained with the **Token/Param**  
 1910 configuration with context length  $T = 8192$ .  
 1911

#Params (M)	$d_{\text{model}}$	$d_{\text{ff}}$	$d_{\text{hv}}$	$n_{\text{heads}}$	$n_{\text{layer}}$	$B$ (seqs)	LR
162	768	2048	64	12	12	128	3e-3, 1e-3
406	1024	2752	64	16	24	128	3e-3, 1e-3
834	1536	4096	96	16	24	256	1e-3
1420	2048	5504	128	16	24	256	8e-4
2779	2560	6848	80	32	32	512	7e-4
6863	4096	10944	128	32	32	256, 512	5e-4

1919  
 1920  
 1921  
 1922  
 1923  
 1924  
 1925  
 1926  
 1927  
 1928  
 1929  
 1930  
 1931  
 1932  
 1933  
 1934  
 1935  
 1936  
 1937  
 1938  
 1939  
 1940  
 1941  
 1942  
 1943

## E.2 MODEL SIZES AND HYPERPARAMETERS IN IsoFLOP CONFIGURATION

Table 21: List of hyperparameters for xLSTM models trained with the IsoFLOP configuration.

#Params (M)	$d_{\text{model}}$	$d_{\text{ff}}$	$d_{\text{qk}}$	$d_{\text{hv}}$	$n_{\text{heads}}$	$n_{\text{layer}}$
83	512	1408	64	128	4	10
90	512	1408	64	128	4	12
96	512	1408	64	128	4	14
102	512	1408	64	128	4	16
114	640	1728	64	128	5	10
123	640	1728	64	128	5	12
128	640	1728	64	128	5	13
133	640	1728	64	128	5	14
143	640	1728	64	128	5	16
164	768	2112	64	128	6	12
185	768	2112	64	128	6	15
207	896	2432	64	128	7	12
207	768	2112	64	128	6	18
236	896	2432	64	128	7	15
265	896	2432	64	128	7	18
295	896	2432	64	128	7	21
324	896	2432	64	128	7	24
330	1024	2752	128	256	4	18
353	896	2432	64	128	7	27
368	1024	2752	128	256	4	21
406	1024	2752	128	256	4	24
444	1024	2752	128	256	4	27
482	1024	2752	128	256	4	30
503	1152	3136	64	128	9	24
552	1152	3136	64	128	9	27
601	1152	3136	64	128	9	30
604	1280	3456	128	256	5	24
664	1280	3456	128	256	5	27
715	1408	3776	64	128	11	24
724	1280	3456	128	256	5	30
787	1408	3776	64	128	11	27
841	1536	4160	128	256	6	24
859	1408	3776	64	128	11	30
927	1536	4160	128	256	6	27
1013	1536	4160	128	256	6	30
1108	1792	4800	128	256	7	24
1224	1792	4800	128	256	7	27
1340	1792	4800	128	256	7	30
1421	2048	5504	128	256	8	24
1573	2048	5504	128	256	8	27
1772	2304	6208	128	256	9	24
1876	2048	5504	128	256	8	33
1964	2304	6208	128	256	9	27
2028	2048	5504	128	256	8	36
2157	2304	6208	128	256	9	30
2350	2304	6208	128	256	9	33
2781	2560	6848	128	256	10	32
3017	2560	6848	128	256	10	35
3150	2816	7552	128	256	11	30
3254	2560	6848	128	256	10	38
3342	2816	7552	128	256	11	32
3533	2816	7552	128	256	11	34
3724	2816	7552	128	256	11	36
3726	3072	8256	128	256	12	30
3954	3072	8256	128	256	12	32
4410	3072	8256	128	256	12	36
4597	3328	8896	128	256	13	32
5130	3328	8896	128	256	13	36
5311	3584	9600	128	256	14	32
5930	3584	9600	128	256	14	36
6464	4096	10944	128	256	16	30
6867	4096	10944	128	256	16	32

1998  
1999  
2000  
2001  
2002  
2003  
2004  
2005  
2006  
2007  
2008  
2009  
2010  
2011  
2012  
2013  
2014  
2015  
2016  
2017  
2018  
2019  
2020  
2021  
2022  
2023  
2024  
2025  
2026  
2027  
2028  
2029  
2030  
2031  
2032  
2033  
2034  
2035  
2036  
2037  
2038  
2039  
2040  
2041  
2042  
2043  
2044  
2045  
2046  
2047  
2048  
2049  
2050  
2051

Table 22: **List of hyperparameters for Transformer models** trained with the **IsoFLOP** configuration.

#Params (M)	$d_{\text{model}}$	$d_{\text{ff}}$	$d_v$	$n_{\text{heads}}$	$n_{\text{layer}}$
83	512	1408	64	8	10
90	512	1408	64	8	12
96	512	1408	64	8	14
102	512	1408	64	8	16
113	640	1728	64	10	10
128	640	1728	64	10	13
133	640	1728	64	10	14
143	640	1728	64	10	16
162	768	2048	64	12	12
183	768	2048	64	12	15
204	768	2048	64	12	18
207	896	2432	64	14	12
236	896	2432	64	14	15
265	896	2432	64	14	18
294	896	2432	64	14	21
324	896	2432	64	14	24
330	1024	2752	64	16	18
368	1024	2752	64	16	21
406	1024	2752	64	16	24
444	1024	2752	64	16	27
482	1024	2752	64	16	30
498	1152	3072	128	9	24
545	1152	3072	128	9	27
593	1152	3072	128	9	30
604	1280	3456	128	10	24
664	1280	3456	128	10	27
714	1408	3776	128	11	24
723	1280	3456	128	10	30
786	1408	3776	128	11	27
834	1536	4096	128	12	24
858	1408	3776	128	11	30
919	1536	4096	128	12	27
1003	1536	4096	128	12	30
1107	1792	4800	128	14	24
1223	1792	4800	128	14	27
1339	1792	4800	128	14	30
1420	2048	5504	128	16	24
1572	2048	5504	128	16	27
1723	2048	5504	128	16	30
1760	2304	6144	128	18	24
1951	2304	6144	128	18	27
2142	2304	6144	128	18	30
2334	2304	6144	128	18	33